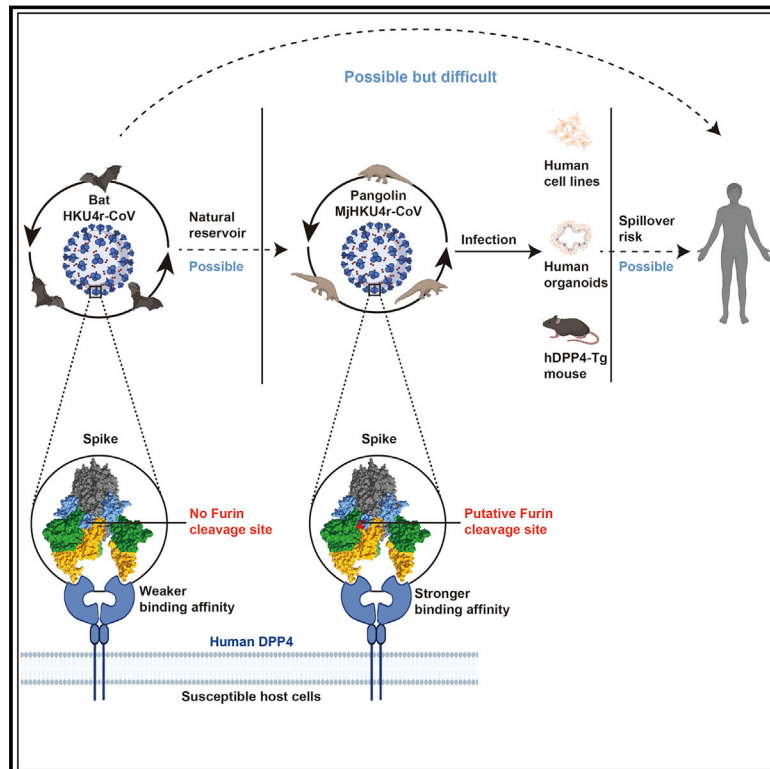


A bat MERS-like coronavirus circulates in pangolins and utilizes human DPP4 and host proteases for cell entry

Graphical abstract



Authors

Jing Chen, Xinglou Yang, Haorui Si, ..., Yanling Hu, Zheng-Li Shi, Peng Zhou

Correspondence

xlin@fudan.edu.cn (X.L.),
tongyigang@mail.buct.edu.cn (Y.T.),
huyanling@gxmu.edu.cn (Y.H.),
zlishi@wh.iov.cn (Z.-L.S.),
peng.zhou@wh.iov.cn (P.Z.)

In brief

A bat MERS-like coronavirus similar to HKU4-CoV is identified circulating in Malayan pangolins. This virus uses human DPP4 as a receptor, bears a furin cleavage site that potentially broadens its host range, and is infectious in human organs and transgenic animals.

Highlights

- A bat HKU4r-CoV (*Merbecovirus*) MjHKU4r-CoV is circulating in Malayan pangolins
- MjHKU4r-CoV-1 uses human DPP4 receptor and can be isolated
- MjHKU4r-CoV-1 has a furin cleavage site and a wider host range than bat HKU4-CoV
- MjHKU4r-CoV-1 is infectious and pathogenic in human organs and hDPP4-Tg mice



Article

A bat MERS-like coronavirus circulates in pangolins and utilizes human DPP4 and host proteases for cell entry

Jing Chen,^{1,11} Xinglou Yang,^{1,11} Haorui Si,^{1,2,11} Qianchun Gong,^{3,4,11} Tengcheng Que,^{5,6,11} Jing Li,^{7,11} Yang Li,¹ Chunguang Wu,^{1,2} Wei Zhang,¹ Ying Chen,^{1,2} Yun Luo,^{1,2} Yan Zhu,¹ Bei Li,¹ Dongsheng Luo,¹ Ben Hu,¹ Haofeng Lin,^{1,2} Rendu Jiang,³ Tingting Jiang,¹ Qian Li,^{1,2} Meiqin Liu,^{1,2} Shizhe Xie,^{1,2} Jia Su,^{1,2} Xiaoshuang Zheng,^{1,2} Ang Li,^{1,2} Yulin Yao,¹ Yong Yang,^{1,2} Panyu Chen,⁵ Aiqiong Wu,⁵ Meihong He,⁵ Xinhua Lin,^{3,4,*} Yigang Tong,^{7,*} Yanling Hu,^{8,9,*} Zheng-Li Shi,^{1,*} and Peng Zhou^{1,10,12,*}

¹CAS Key Laboratory of Special Pathogens, Wuhan Institute of Virology, Chinese Academy of Sciences, Wuhan, China

²University of Chinese Academy of Sciences, Beijing, China

³State Key Laboratory of Genetic Engineering, School of Life Sciences, Greater Bay Area Institute of Precision Medicine (Guangzhou), Zhongshan Hospital, Fudan University Shanghai, Shanghai 200438, China

⁴Joint Laboratory for Lung Development and Related Diseases of West China Second University Hospital, Sichuan University and School of Life Sciences of Fudan University, Chengdu 610041, China

⁵Guangxi Zhuang Autonomous Region Terrestrial Wildlife Medical-aid and Monitoring Epidemic Diseases Research Center, Nanning 530028, Guangxi, China

⁶Faculty of Data Science, City University of Macau, Beijing, China

⁷Beijing Advanced Innovation Center for Soft Matter Science and Engineering, College of Life Science and Technology, Beijing University of Chemical Technology, Beijing, China

⁸Institute of Life Sciences, Guangxi Medical University, Nanning 530021, Guangxi, China

⁹Center for Genomic and Personalized Medicine, Guangxi Key Laboratory for Genomic and Personalized Medicine, Guangxi Collaborative Innovation Center for Genomic and Personalized Medicine, Guangxi Medical University, Nanning 530021, Guangxi, China

¹⁰Guangzhou Laboratory, No. 9 Xing Dao Huan Bei Road, Guangzhou International Bio Island, Guangzhou 51005, Guangdong Province, China

¹¹These authors contributed equally

¹²Lead contact

*Correspondence: xlin@fudan.edu.cn (X.L.), tongyigang@mail.buct.edu.cn (Y.T.), huyanling@gxmu.edu.cn (Y.H.), zishi@wh.iov.cn (Z.-L.S.), peng.zhou@wh.iov.cn (P.Z.)

<https://doi.org/10.1016/j.cell.2023.01.019>

SUMMARY

It is unknown whether pangolins, the most trafficked mammals, play a role in the zoonotic transmission of bat coronaviruses. We report the circulation of a novel MERS-like coronavirus in Malayan pangolins, named *Manis javanica* HKU4-related coronavirus (MjHKU4r-CoV). Among 86 animals, four tested positive by pan-CoV PCR, and seven tested seropositive (11 and 12.8%). Four nearly identical (99.9%) genome sequences were obtained, and one virus was isolated (MjHKU4r-CoV-1). This virus utilizes human dipeptidyl peptidase-4 (hDPP4) as a receptor and host proteases for cell infection, which is enhanced by a furin cleavage site that is absent in all known bat HKU4r-CoVs. The MjHKU4r-CoV-1 spike shows higher binding affinity for hDPP4, and MjHKU4r-CoV-1 has a wider host range than bat HKU4r-CoV. MjHKU4r-CoV-1 is infectious and pathogenic in human airways and intestinal organs and in hDPP4-transgenic mice. Our study highlights the importance of pangolins as reservoir hosts of coronaviruses poised for human disease emergence.

INTRODUCTION

The animal origin and zoonotic transmission cycle of important coronaviruses (CoVs) that have caused human outbreaks, such as SARS, MERS, and COVID-19, are not fully understood. As natural reservoir hosts, bats carry a large diversity of CoVs of the subgenera *Sarbecovirus* and *Merbecovirus* that may be related to the three outbreaks.¹ Therefore, it is generally believed

that SARS-CoV and SARS-CoV-2, the etiological agents of SARS and COVID-19, respectively, have bat origins.^{2,3} Bats have also been suggested as the source of MERS-CoV, which emerged in Middle Eastern countries in 2012.⁴

However, bats and humans rarely come into physical contact, and bat CoVs normally require further adaptation before they can directly infect or replicate in human cells, suggesting a requirement for an intermediate animal host.^{5–10} Game animals, which



are wildlife species traded and consumed as food, such as civets and hedgehogs, are believed to be potential drivers of disease emergence in humans as intermediate hosts. As the most trafficked game mammals, pangolins may play an important role in the ecology of CoVs as suggested by the identification of two CoV lineages phylogenetically related to SARS-CoV-2 from smuggled Malayan pangolins (*Manis javanica*) in Guangdong and Guangxi, China.^{11,12} Importantly, these two viruses, termed Pangolin-CoV-GD and -GX, were isolated and demonstrated to efficiently use human ACE2 as a receptor and replicate in human cells, suggesting a high risk of zoonotic transmission to humans.^{12–14} Furthermore, partial sequences similar to the Pangolin-CoV-GX sequence were detected in archived samples of Malayan pangolin and Chinese pangolin (*Manis pentadactyla*) smuggled to China from Southeast Asia in 2017.¹⁵ Serological data, although from a limited number of samples, have indicated that infection of pangolins by SARS-related CoVs can be traced back to 2003.¹⁶ The limited information regarding the pangolin virome shows that these animals carry a number of unidentified viruses, including CoVs.¹⁷

In contrast to the general perception of the role played by game animals in CoV spillover from bats to humans, there is still limited evidence for the circulation of bat-related CoVs in game animals and limited virological evidence to show that the viruses in game animals are more human adapted than bat CoVs. This study showed that pangolins carry pre-emergent MERS-like CoVs that are related to bats but are capable of direct infection and show enhanced infectivity to humans compared with the bat viruses, indicating the important role of pangolins in CoV emergence in humans.

RESULTS

Identification of a MERS-like CoV related to *Tylonycteris* bat CoV HKU4 (HKU4-CoV) from Malayan pangolins

A total of 86 anal swab samples from Malayan pangolins that were illegally smuggled into China from Southeast Asia were screened by pan-CoV PCR targeting the RNA-dependent RNA polymerase (*RdRp*) gene, yielding four CoV-positive test results. Using next-generation sequencing (NGS), we identified a novel MERS-like CoV that is phylogenetically related to bat HKU4-CoV. Through metagenomics *de novo* assembly, rapid amplification of cDNA ends (RACE), and Sanger sequencing, we obtained four nearly identical full-length CoV genomes of 30,340 bp in length from these four samples, which we termed *Manis javanica* HKU4-related coronavirus 1–4 (MjHKU4r-CoV-1–4) (Figure S1A). MjHKU4r-CoV-1 shows a typical *Merbecovirus* genome structure and contains all 10 viral open reading frames (ORFs) present in the subgenus *Merbecovirus* (Figure 1A).⁴ According to the latest classification, this subgenus comprises MERS-related CoVs from humans, camels, and bats, HKU4-CoV, *Pipistrellus* bat CoV HKU5 (HKU5-CoV), and Hedgehog CoV 1 from *Erinaceus europaeus* (EriCoV).¹⁸ Further analysis indicated that MjHKU4r-CoV-1 shares 67.9% and 86.8% genome identity with MERS-CoV and HKU4-CoV, respectively (Table S1). Similarity plot analysis showed that MjHKU4r-CoV-1 exhibits the highest genome nucleotide identity to bat HKU4-CoV, which was consistent with the results of iden-

tity comparison of the individual genes (Figure 1B; Table S1). Recombinant analysis showed no recombinant event in the MjHKU4r-CoV-1 genome sequence. MjHKU4r-CoV-1–4 form a distinct lineage within HKU4r-CoVs based on the full-length genome and the *RdRp* and spike (S) genes (Figures 1C, S1B, and S1C). In the seven conserved replicase domains of ORF1ab that were used for CoV species classification, MjHKU4r-CoV-1 shares 96.1% amino acid identity to HKU4-CoV (BtTp-BetaCoV/GX2012), indicating that it belongs to the species *Tylonycteris bat coronavirus HKU4*, subgenus *Merbecovirus* (Table S1).

The above results suggested the circulation of MjHKU4r-CoV in pangolins. To investigate its prevalence, we developed an antibody assay based on the MjHKU4r-CoV-1 nucleocapsid protein (NP), using a luciferase immunoprecipitation system (LIPS).¹⁹ Among 80 serum samples collected from the same batch of pangolins, another seven animals tested seropositive for MjHKU4r-CoV by the LIPS assay. Moreover, the serum sample that showed the strongest seropositivity also showed MjHKU4r-CoV-1 neutralizing activity (Figures S2A–S2C). Thus, at least 11 out of 86 (12.8%) pangolins were MjHKU4r-CoV positive.

MERS-CoV uses human dipeptidyl peptidase-4 (hDPP4) as a cell-entry receptor, and cell membrane fusion is mediated by proteolytic cleavage of its S protein by host proteases, a process that can be enhanced by furin protease.²⁰ There are 16 key residues in the receptor-binding motif (RBM) of the MERS-CoV S protein that determine the binding with hDPP4.²¹ MjHKU4r-CoV-1 shares eight of these 16 key residues, suggesting that it may also use hDPP4 as cell-entry receptor. As a comparison, bat HKU4-CoV, which uses hDPP4 as a receptor,^{22,23} shares seven out of 16 contact residues with MERS-CoV, whereas HKU5-CoV, which shares only one residue, does not bind to hDPP4.²² In addition, we predicted a potential furin protease cleavage site (RQQR) in S protein subdomain 1 (SD1) in all MjHKU4r-CoV genomes that is similar to that in the MERS-CoV genome and believed to play an important role in SARS-CoV-2 transmission.²⁴ However, such a cleavage site was not found in any of the publicly available bat HKU4r-CoV genomes (Figures 1D and S3).

Isolation of MjHKU4r-CoV-1 and elucidation of its cell-entry mechanism

We successfully isolated MjHKU4r-CoV-1 in Caco-2 cells from a pangolin anal swab sample. Clear cytopathogenic effects were observed at 5 days after inoculation. In electron microscopy, viral particles displayed typical CoV morphology, with a diameter of approximately 100 nm (Figure 2A). The isolation of MjHKU4r-CoV-1 was confirmed by positive immunofluorescence staining of NP in Caco-2 cells (Figure 2B), a viral load increase from day 0 to day 3, and the enrichment of virus reads in a metagenomics analysis of cell culture supernatant (Figure 2C). No sequence change was observed in the cultured MjHKU4r-CoV-1 genome compared with the original MjHKU4r-CoV-1 genome (Figure S4).

Receptor usage and S protein cleavage are two barriers to merbecovirus infection in human cells.²⁵ Given that both MERS-CoV and bat HKU4-CoV use hDPP4 as a cell-entry

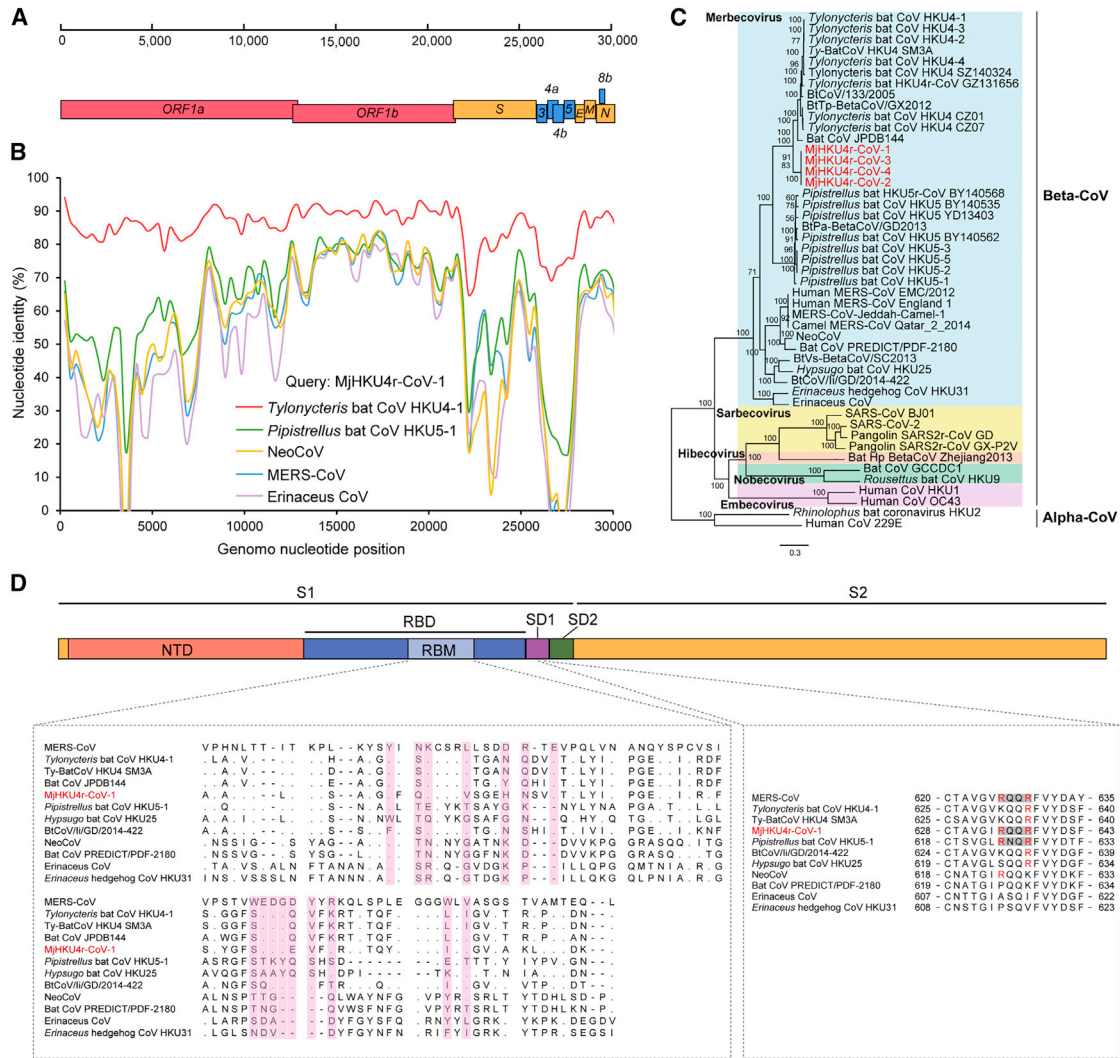


Figure 1. Genome characteristics of pangolin MERS-like CoV, *Manis javanica* HKU4-related CoV (MjHKU4r-CoV)

(A) Genome structure of MjHKU4r-CoV-1.

(B) Similarity plot based on the full-length genome sequences. MjHKU4r-CoV-1 was used as a query sequence, *Tylonycteris* bat CoV HKU4-1, *Pipistrellus* bat CoV HKU5-1, bat MERS-related NeoCoV, and human MERS-CoV were used as reference sequences.

(C) Phylogenetic tree based on the nucleotide sequences of the complete genomes of representative Alpha coronavirus (Alpha-CoV) and Beta coronavirus (Beta-CoV). MjHKU4r-CoV-1–4 are shown in red. Shaded colors represent different subgenera of coronaviruses. The scale bars represent 0.3 substitutions per nucleotide position. The software and setting used are described in the STAR Methods.

(D) Schematic representation of the S protein. S1 and S2 subunits are indicated, as well as four domains within S1, including the N-terminal domain (NTD), RBD, subdomain 1 (SD1), and subdomain 2 (SD2). RBM alignment is shown at the bottom left, and the 16 key residues situated at the surface between MERS-CoV RBM and human DPP4 are pink shaded. Predicted furin cleavage sites of MjHKU4r-CoV-1 and the corresponding sites in other merbecoviruses are shown at the bottom right. The key arginine sites are shown in red, and the predicted furin cleavage sites are gray shaded.

See also Figures S1, S2, and S3 and Table S1.

receptor,^{23,26} we questioned whether MjHKU4r-CoV-1 uses hDPP4 for entry as well. We inoculated human Huh-7 cells with or without DPP4 expression with MjHKU4r-CoV-1 or MERS-CoV (as a positive control). MjHKU4r-CoV-1 and MERS-CoV infections were nearly completely abolished in *DPP4*-knockout Huh-7 cells (Figures 2D–2G) and were successfully restored when hDPP4 was re-introduced by overexpression (Figures 2H–2K). These data indicated that MjHKU4r-CoV-1 uses hDPP4 as a cell-entry receptor.

We next determined whether MjHKU4r-CoV-1 can cross the proteolytic cleavage barrier. We found that viral infection was largely suppressed in Huh-7 cells pretreated with E64D, an inhibitor of cysteine-class proteases, including endosomal cathepsins, but was barely affected by pretreatment with camostat, an inhibitor of serine-class transmembrane proteins. Importantly, exogenous trypsin was found to not be necessary for MjHKU4r-CoV-1 infection, suggesting that this virus is fully adapted to proteolytic cleavage in human cells.

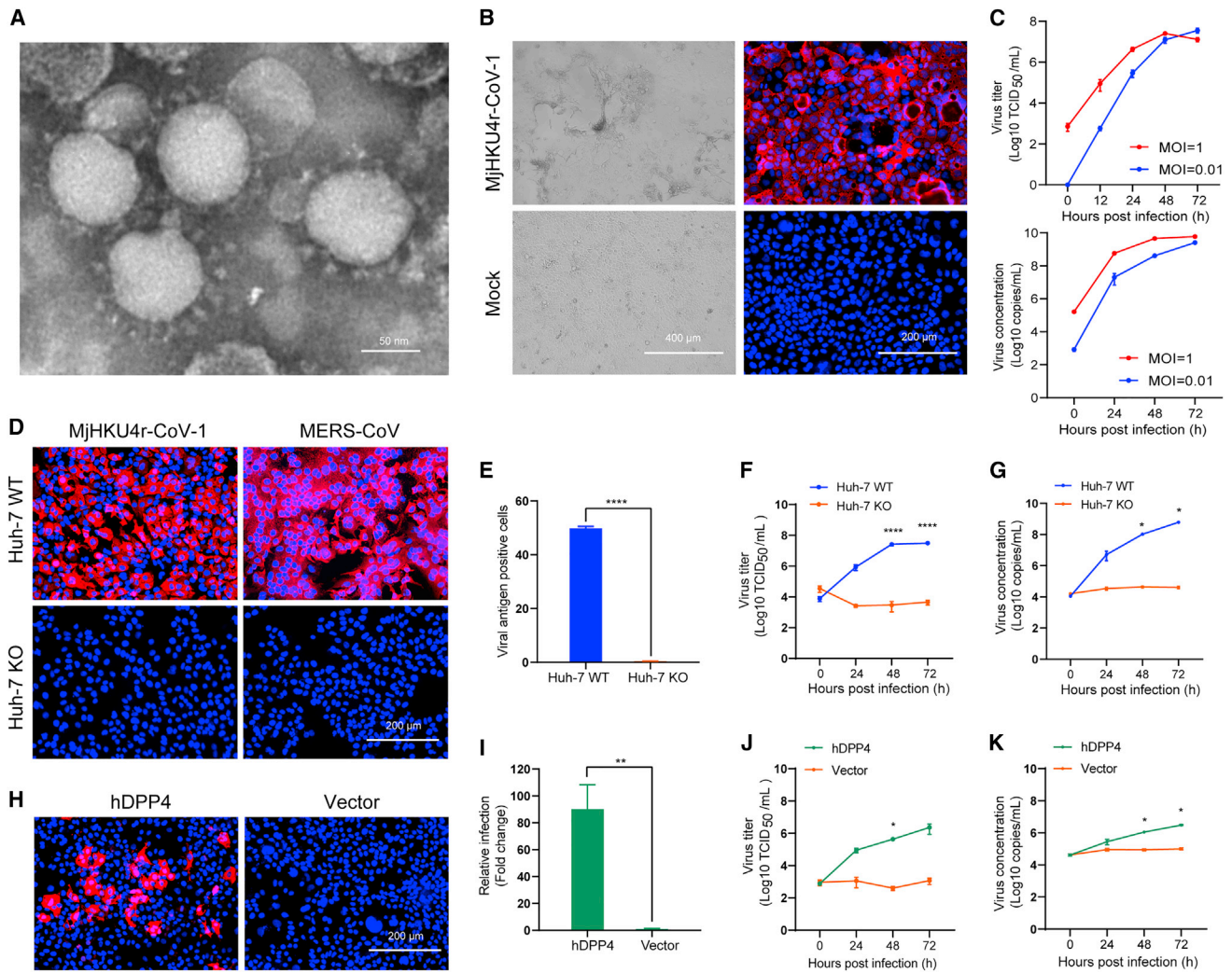


Figure 2. Isolation of MjHKU4r-CoV-1 and elucidation of its cell-entry mechanism

(A) Transmission electron microscopy analysis of MjHKU4r-CoV-1 virions. Scale bars, 50 nm. (B) Cytopathic effect in Caco-2 cells at 48 h.p.i. with MjHKU4r-CoV-1 or mock infected (left, scale bars, 400 μ m), and immunofluorescence assay (IFA) with an antibody against the *Tylosyncytis* bat coronavirus HKU4 NP (right, scale bars, 200 μ m). Red, NP; blue, nuclei. (C) Caco-2 cells were infected with MjHKU4r-CoV-1 at a multiplicity of infection (MOI) of 1 or 0.01. Viral titers and viral RNA copies at indicated time points were determined by TCID₅₀ assay and qRT-PCR, respectively. (D–G) Viral infection in Huh-7 cells with or without hDPP4 expression. Wild-type (WT) or *DPP4*-knockout Huh-7 (KO) cells were infected with MjHKU4r-CoV-1 or MERS-CoV for 24 h. IFA was performed (D, scale bars, 200 μ m) and quantified by high content screening (E), and viral titer (F) and RNA copy number (G) were determined in the supernatant. (H–K) Viral infection in KO cells after hDPP4 re-introduction. IF staining in Huh-7 KO cells transfected with hDPP4 expression plasmid or empty vector (H, scale bars, 200 μ m) quantified by high content screening (I), and viral titer (J) and RNA copies (K) were determined in the supernatant at the indicated times. Data are presented as means and standard errors of the means (SEMs) of at least triplicate measurements in (E–G and I–K). Statistical significance was assessed using a two-tailed Student's *t*-test in (E and I) and two-way ANOVA in (F, G, J, and K). See also Figure S4.

Addition of the furin inhibitor decanoyl-Arg-Val-Lys-Arg-chloromethyl ketone (decRVKRCmk) significantly suppressed MjHKU4r-CoV-1 infection in Huh-7 cells, suggesting that it depends on furin cleavage as well (Figures 3A and 3B). To corroborate the finding of a potential furin cleavage site in MjHKU4r-CoV-1, but not in the bat HKU4-CoV S protein, we assessed whether point mutation in the predicted furin cleavage site would dampen proteolytic S protein cleavage and viral infection. Con-

structs encoding the wild-type MjHKU4r-CoV-1 S protein and a mutant S protein carrying a RQQR to AQQA substitution (aa 634–637) were generated (Figures 3C and 3D). Proteolytic cleavage was observed for the wild-type MjHKU4r-CoV-1 and MERS-CoV S proteins. In contrast, no obvious cleavage was observed for mutant MjHKU4r-CoV-1 and HKU4-CoV S proteins (Figure 3E). Consistent herewith, viral entry was hampered by the point mutations in pseudotyped particles (Figures 3F and 3G),

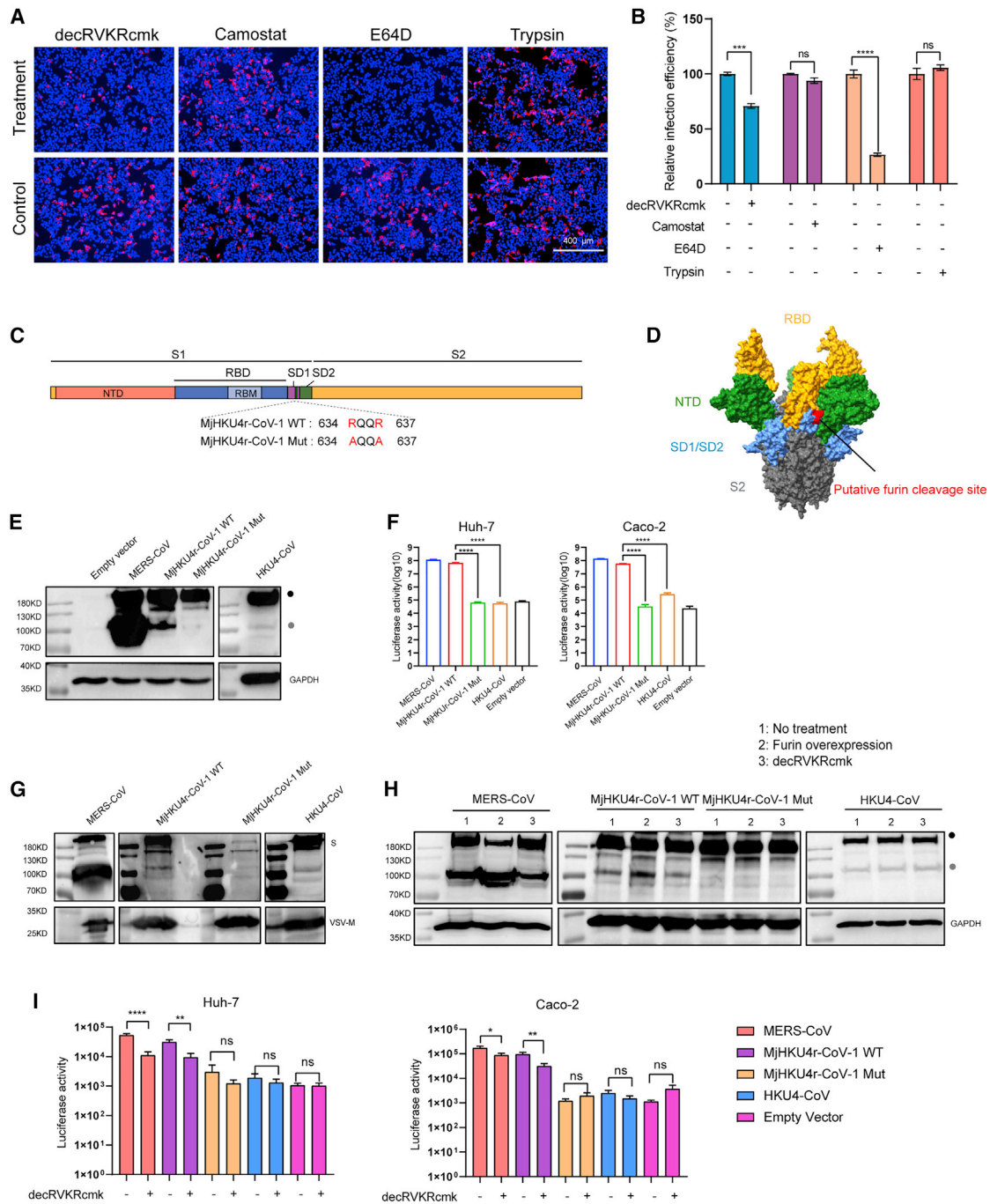


Figure 3. Effect of host protease on viral entry and S protein cleavage of MjHKU4r-CoV-1

(A and B) Proteolytic cleavage dependency in human cells. Huh-7 cells were pretreated with the indicated protease inhibitors or exogenous trypsin for 2 h before infection with MjHKU4r-CoV-1 at a MOI of 10. Cells were stained by IFA at 8 h.p.i. The cells were pretreated with 10 μ M furin inhibitor decRVKRcmk or water as a control; 50 μ M serine-class protease inhibitor camostat or 0.5% dimethylsulfoxide (DMSO) as control; 50 μ M cysteine-class protease inhibitor E64D or 0.1% DMSO as a control; or 0.5 μ g/mL trypsin or Dulbecco's modified Eagle's medium (DMEM) as control. Data are shown as IF images (A, scale bars, 400 μ m) or IF quantification (B).

(C) Mutations introduced into the potential furin cleavage site in MjHKU4r-CoV-1 S protein.

(D) Structure model for MjHKU4r-CoV-1 S protein predicted based on the PDB: 5X5C structure as a template using the SWISS-MODEL online tool (swissmodel.expasy.org). The predicted furin cleavage site is shown in red.

(legend continued on next page)

which have been observed for MERS-CoV.^{20,26,27} These data suggested that the MjHKU4r-CoV-1 S protein is cleaved by a host protease during biosynthesis, and this cleavage is critical for virus entry. To determine whether this cleavage is furin specific, experiments using a furin inhibitor or furin overexpression were performed. The results showed that MjHKU4r-CoV-1 and MERS-CoV S protein cleavage was enhanced by furin overexpression but suppressed by furin inhibitor treatment. Similarly, pseudovirus entry was suppressed in the presence of the furin inhibitor. Under these conditions, there was no detectable change in the proteolytic cleavage of mutant MjHKU4r-CoV-1 or HKU4-CoV S protein or pseudovirus (Figures 3H and 3I). Taken together, these data indicated that pangolin MjHKU4r-CoV-1 carries a specific furin cleavage site (most probably, RQQR) that is not found in bat HKU4-CoV.

Thus, MjHKU4r-CoV-1 uses hDPP4 and human proteolytic proteases cleavage for infecting human cells, indicating that this virus is capable of directly infecting human cells without the need for further adaptation.

The MjHKU4r-CoV-1 RBD binds to human, bat, and pangolin DPP4

Given the genetic relationships between MjHKU4r-CoVs and bat HKU4r-CoVs, we next determined whether MjHKU4r-CoV-1 potentially infects humans and bats based on receptor usage. We found that MjHKU4r-CoV-1 effectively infected cells overexpressing *Tylonycteris pachypus* (*Tp*) bat DPP4, *Pipistrellus* (*Pp*), of the same genus as the reservoir host of HKU5-CoV) bat DPP4, *Mj* pangolin DPP4, and human DPP4, without prominent differences (Figure 4A). To corroborate these findings, we compared the binding affinities of the MjHKU4r-CoV-1 receptor-binding domain (RBD) to a series of DPP4 proteins with that of MERS-CoV or bat HKU4-CoV RBD as a control. The results showed that the MjHKU4r-CoV-1 RBD has binding affinity to human, bat, and pangolin DPP4. In contrast, the MERS-CoV RBD showed binding affinity to human and *Tp* bat DPP4, but not to other DPP4s (*Pp* bat and *Mj* pangolin), whereas the HKU4-CoV RBD showed binding affinity only to *Tp* bat DPP4 and hDPP4 (very weak). Notably, the binding affinity between the MjHKU4r-CoV-1 RBD and hDPP4 was close to that between the MERS-CoV RBD and hDPP4 (Figure 4B; Table S2).

To determine the potential host range of MjHKU4r-CoV-1, we assessed DPP4 receptor usage in multiple mammals. The data demonstrated that MjHKU4r-CoV-1 infection can also be mediated by DPP4 orthologs from pigs, goats, cats, rabbits, macaques, sheep, camels, marmosets, and cattle, but not from ferrets, horses, rats, hamsters, dogs, and mice (Figure S5). Thus, MjHKU4r-CoV-1 appears to have a wide host infection spectrum, similar to that of MERS-CoV, in terms of receptor usage.

MjHKU4r-CoV-1 replicates in human respiratory and intestinal organoids

The respiratory and enteric tracts are the two primary target organs of CoVs for replication and transmission.¹ The identification of MjHKU4r-CoV-1 and its ability to use human DPP4 and cleavage proteases for infection highlighted its potential risk for human emergence. To test this possibility, we developed a framework to examine MjHKU4r-CoV-1 infection in multiple human cell lines, organoids, and *ex vivo* organs. MjHKU4r-CoV-1 efficiently infected and replicated in human cell lines A549, Calu-3, Caco-2, HEK293, and Huh-7 cells after a 72-h culture, suggesting a wide tissue tropism of this virus (Figure S6A). Further, MjHKU4r-CoV-1 replicated in human colon organoids, with a substantially increased viral load of more than 6 log units in the culture medium and 3 log units in cells at 72 h post infection (h.p.i.) (Figures 5A–5C). Viral infection and the co-localization of viral NP-positive cells with DPP4-positive cells were verified by immunofluorescence staining (Figure 5D). Similar observations were made in primary human airway organoids and *ex vivo* human colon tissues (Figures 5E–5H and S6B–S6D).

MjHKU4r-CoV-1 infection induces pathological injury in hDPP4-Tg mouse lungs

To better understand the human infection potential and pathogenicity of MjHKU4r-CoV-1, we conducted *in vivo* infection experiments in hDPP4-transgenic (Tg) mice. hDPP4-Tg mice were intranasally infected with 1×10^6 50% tissue culture infectious dose (TCID₅₀) MjHKU4r-CoV-1 and monitored for 8 days. Mice infected with MjHKU4r-CoV-1 showed minimal body weight loss, but no lethality (Figures 6A and 6B). MjHKU4r-CoV-1 maintained replicating infection in the lungs of some of the infected

(E) Western blot analysis of S protein cleavage products during protein biosynthesis. HEK293 cells were transfected with MERS-CoV, wild-type MjHKU4r-CoV-1, mutant MjHKU4r-CoV-1, or bat HKU4-CoV S protein expression plasmid containing a C-terminal S-tag. Empty vector transfection served as a negative control. At 48 h.p.t., the cells were harvested, lysed, and subjected to western blotting using the anti-S-tag antibody. S protein and cleaved S are indicated with point markers.

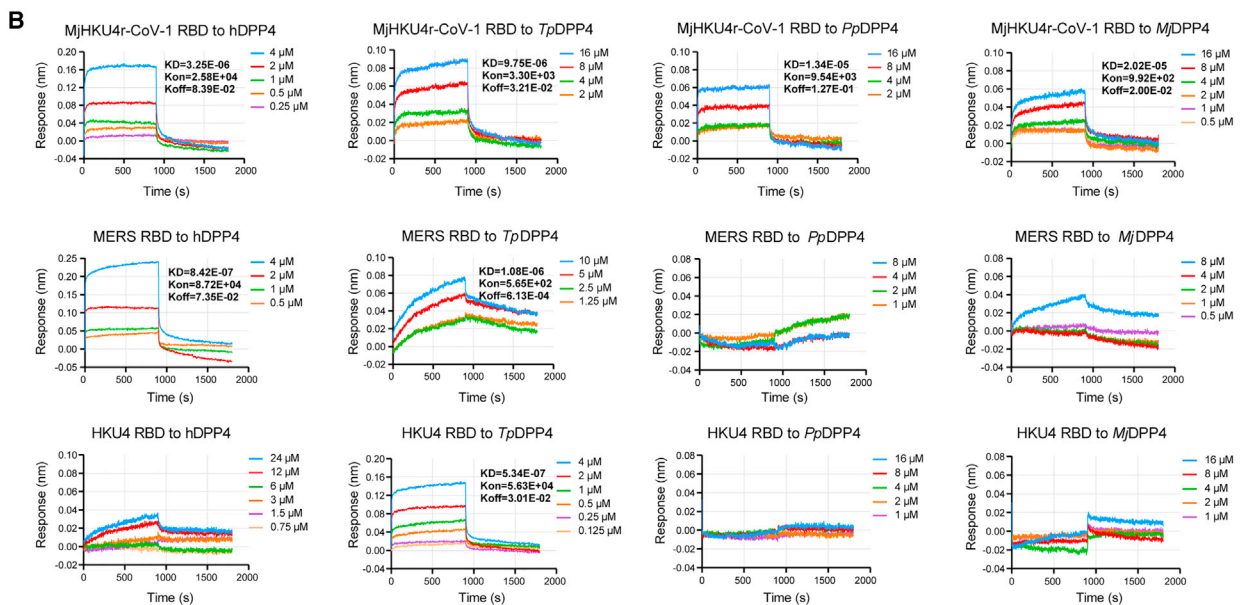
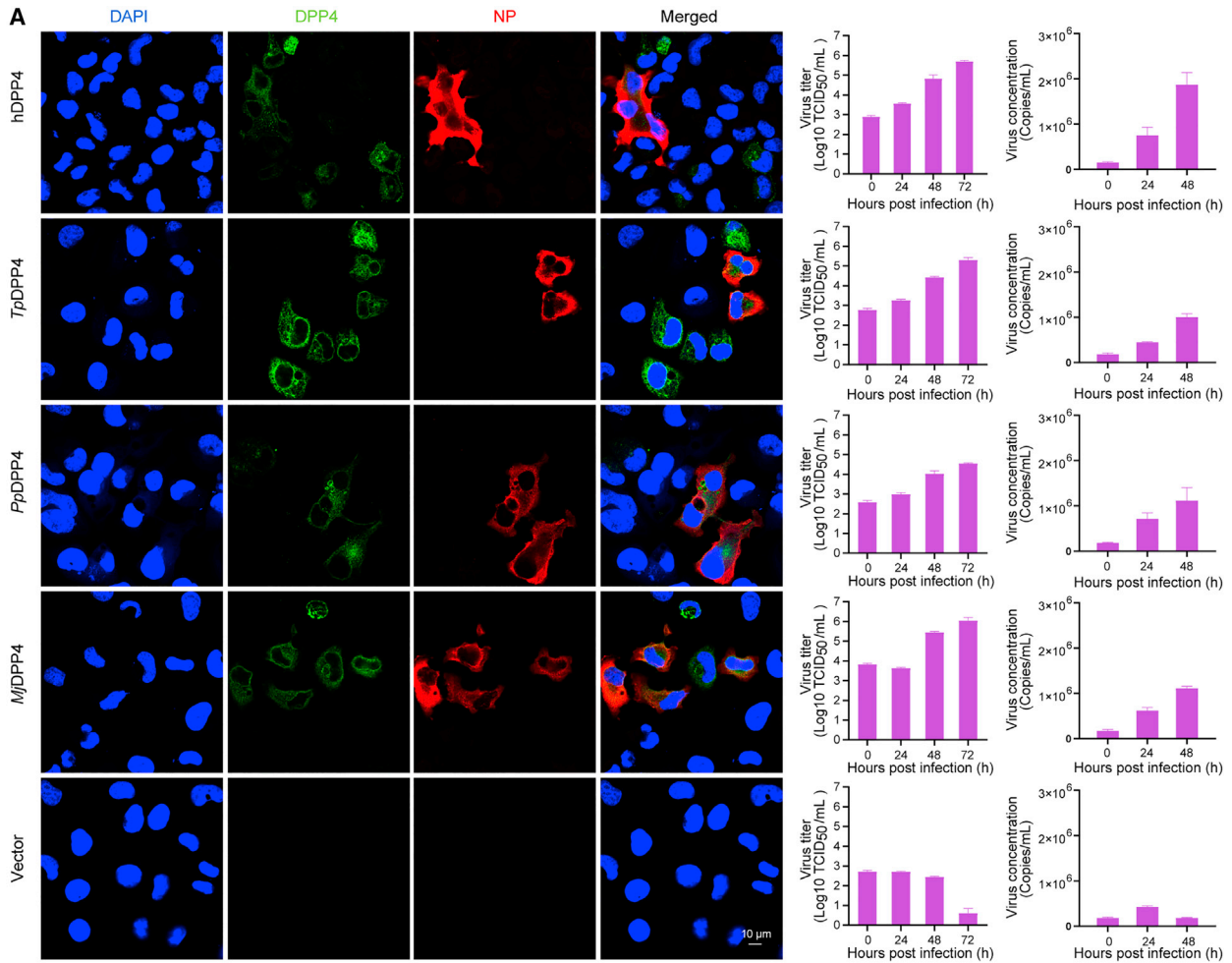
(F) Huh-7 and Caco-2 cells were infected with pseudoviruses harboring MERS-CoV, wild-type MjHKU4r-CoV-1, mutant MjHKU4r-CoV-1, or HKU4-CoV S protein carrying a detectable luciferase. Entry efficiency was compared by measuring luciferase activity.

(G) Analysis of pseudovirus package. Medium containing pseudovirions harboring MERS-CoV, wild-type MjHKU4r-CoV-1, mutant MjHKU4r-CoV-1, or HKU4-CoV S protein was harvested and ultra-centrifuged, followed by western blot analysis. Detection of vesicular stomatitis virus matrix protein (VSV-M) served as control.

(H) Analysis of furin-mediated S protein processing. MERS-CoV, wild-type MjHKU4r-CoV-1, mutant MjHKU4r-CoV-1, or HKU4-CoV S protein expression plasmid was co-transfected with empty vector or furin expression plasmid into HEK293 cells in the presence or absence of a furin inhibitor (10 μ M decRVKRcmk). At 48 h.p.t., the cells were lysed, and S protein cleavage was analyzed by western blotting using the anti-S-tag antibody. S protein and cleaved S are indicated with point markers.

(I) Effect of furin cleavage on viral entry mediated by S protein. MERS-CoV, wild-type MjHKU4r-CoV-1, mutant MjHKU4r-CoV-1, or bat HKU4 pseudovirus was produced in the presence or absence of a furin inhibitor (10 μ M decRVKRcmk) and used to infect Huh-7 cells or Caco-2 cells. Viral entry was quantified by measuring luciferase at 48 h.p.i.

Data are presented as means and SEMs of at least triplicate measurements in (B, F, and I). Statistical significance was assessed using a two-tailed Student's t test.



(legend on next page)

mice for 8 days, and viral NP was detected in bronchial epithelial and alveolar cells at 5 days post infection (d.p.i.) (Figures 6C and 6E). Notably, MjHKU4r-CoV-1 RNA and NP were also detected in the brains (Figures 6D and 6E). Pathological analysis revealed that MjHKU4r-CoV-1 infection resulted in mild to moderate interstitial pneumonia from 5 d.p.i., characterized by peribronchiolar and perivascular inflammation, intravascular thrombosis, thickened alveolar septa, alveolar damage, and focal fibrin exudation (Figure 6F). Taken together, these data indicate that MjHKU4r-CoV-1 is infectious and induces histological injury in mice.

Highly pathogenic CoVs harbor genes encoding interferon (IFN) antagonist activity and early host innate immunity escape, such as ORF4a/4b in MERS-CoV, which contribute to their pathogenesis in humans.²⁸ We found that MjHKU4r-CoV-1 infection induced an overt but delayed IFN response in Caco-2 cells, suggesting that host IFN response escape by this virus (Figures S7A–S7D). To determine the virally encoded IFN antagonists, we evaluated the effect of various structural and accessory proteins on type I IFN production and signaling. The results revealed that the expression of S, M, ORF3, and ORF4a significantly inhibited IFN- β promoter activation, while M, N, ORF3, ORF4a, ORF4b, and ORF8b proteins significantly inhibited type I IFN-stimulated response element (ISRE) promoter activity (Figures S7E and S7F).

Potential therapeutics for MjHKU4r-CoV-1 infection

Finally, we sought to determine whether known therapeutics are effective against MjHKU4r-CoV-1, in preparation for the potential future emergence of this virus. Small molecules, such as GC376, remdesivir, and EIDD-2801, have been demonstrated to inhibit the replication of various viruses.^{29–31} Sequence analysis revealed that MjHKU4r-CoV-1 non-structural protein (nsp) 5 (target of GC376) and nsp12 (target of remdesivir and EIDD-2801) are conserved, while the drug target sites are even identical among MjHKU4r-CoV-1, MERS-CoV, and SARS-CoV-2, suggesting that GC376, remdesivir, and EIDD-2801 exert antiviral activity against MjHKU4r-CoV-1 (Figures 7A and 7B). Our data showed that all three small molecules suppressed MjHKU4r-CoV-1 infection to comparable degrees to MERS-CoV infection at the same concentrations (Figures 7C and 7D). Subsequently, we tested three human-derived monoclonal antibodies, m336, ZME2711, and ZME07117, which show good neutralizing activity against MERS-CoV.³² The antibodies showed no or only background levels of neutralizing activity against MjHKU4r-CoV-1 (Figures 7E and 7F). The low neutralizing activity of m336 toward MjHKU4r-CoV-1 can be explained by the very few amino acid identical to MERS-CoV in the m336-binding sites in the S protein (Figure 7G).

DISCUSSION

We report the circulation of a novel MERS-like CoV in Malayan pangolins. For cell entry, pangolin MjHKU4r-CoV-1 utilizes human DPP4 and human proteolytic cleavage proteases, including furin, almost as efficiently as MERS-CoV. MjHKU4r-CoV is infectious and pathogenic in the human airways and intestinal organs, as well as in hDPP4-Tg mice. Our study highlights the MERS-like virus potentially emerges in humans and the importance of pangolins as reservoir hosts of CoVs poised for human emergence, including at least *Sarbecovirus*^{11,12} and *Merbecovirus*. The prevalence of this virus related to bats but more adapted to humans in pangolins suggests the latter to be important or even adaptation hosts during bat CoV cross-species transmission.

It has been suggested that the risk of spillover is greater when there are more opportunities for human-animal contact, for example, during deforestation or in the trade of wildlife, as these animals are important natural virus reservoir hosts.³³ For instance, bats carry the most CoV species, followed by small mammals, such as rodents, shrews, hedgehogs, civets, and pangolins. Compared with bats, small mammals that are frequently traded pose a bigger threat to humans in terms of CoV spillover. The 2002 human SARS-CoV-1 spillover could have been interrupted if the prevalence and virological assessment of civet SARS-CoV-1, which was related to bat SARS-related CoV, would have been determined early, before it jumped to humans. In this regard, our data provide a novel insight that game animals such as pangolins could be more human-threatening reservoir hosts than bats because they are in closer contact with humans and carry more human-adapted CoVs, and early investigation may break the chain of viral cross-species transmission.

The genetic relationship and divergence between the MjHKU4r-CoVs and bat HKU4r-CoVs suggest a possible bat-pangolin transmission of this virus species, which was occurred a long time ago. It remains unclear whether pangolins are infected by zoonotic transmission directly from bats or from other mammals in the trade chain. Compared with bat HKU4r-CoVs, MjHKU4r-CoVs appear to be better adapted to humans. The emergence and high transmissibility of SARS-CoV-2 variants are largely attributed to an additional furin cleavage site, which is not observed in other sarbecoviruses, and a higher ACE2-binding capacity in later variants.²⁴ Similarly, although bat HKU4r-CoVs have been isolated and could infect hDPP4-Tg mice, they generally show poor receptor-binding capacity or sometimes require exogenous trypsin treatment for human cell entry, indicating the requirement for further adaptation in human cells.^{22,23,26,34} In contrast, MjHKU4r-CoVs utilize hDPP4 (as efficiently as MERS-CoV) and human proteolytic cleavage

Figure 4. MjHKU4r-CoV-1 binds to human, bat, and pangolin DPP4 proteins

(A) HeLa cells overexpressing the following DPP4 orthologous: hDPP4, *Tylonycteris pachypus* bat DPP4 (TpDPP4), *Pipistrellus* bat DPP4 (PpDPP4), or *Manis javanica* DPP4 (MjDPP4) were infected with MjHKU4r-CoV-1 at a MOI of 1 and subjected to IF staining at 24 h.p.i. Shown as MjHKU4r-CoV-1 NP or DPP4 protein expression (left, scale bars, 10 μ m), or the replication dynamics of MjHKU4r-CoV-1 (viral titer, middle panel; genomic RNA, right panel). For IF staining, green, DPP4; red, NP; blue, nuclei.

(B) Binding affinity of MjHKU4r-CoV-1, MERS-CoV, and HKU4r-CoV RBD proteins to human, bat, and pangolin DPP4 proteins as measured by Bio-layer interferometry assay. The quantification of the binding affinity is shown in Table S2.

See also Figure S5 and Table S2.

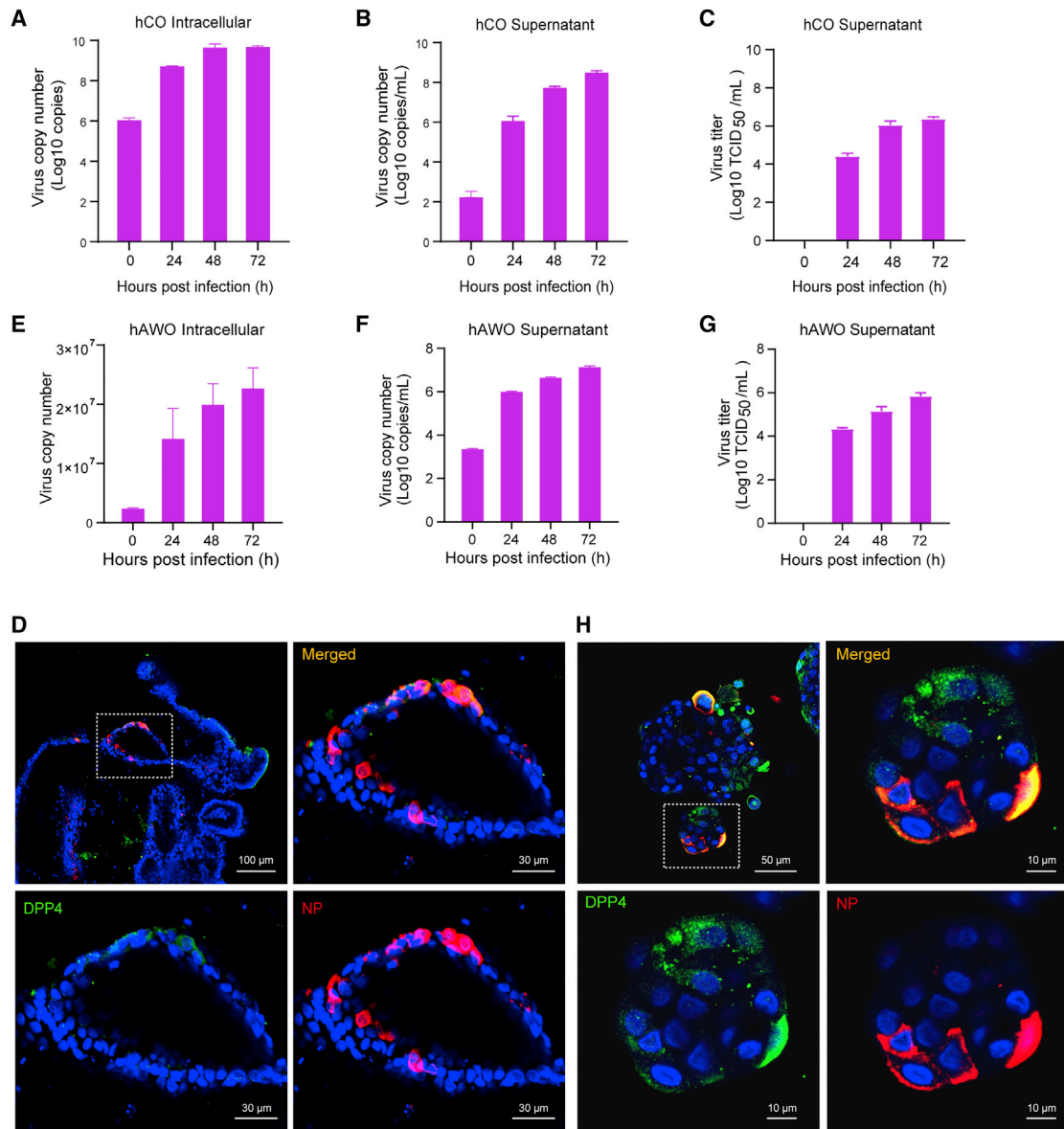


Figure 5. MjHKU4r-CoV-1 infection in human colon organoids and airway organoids

(A–C) Replication of MjHKU4r-CoV-1 in human colon organoids (hCO), shown as viral copy numbers in cells (A) and supernatants (B) and viral titers in supernatants (C) as analyzed by qRT-PCR and TCID₅₀ assay, respectively.

(D) Co-staining of MjHKU4r-CoV-1 NP (red) and hDPP4 (green) in human colon organoids at 72 h.p.i. (scale bars, 100 or 30 μ m). Blue, nuclei.

(E–G) Replication of MjHKU4r-CoV-1 in human airway organoids (hAWOs), shown as viral copy numbers in cells (E) and supernatants (F) and viral titers in supernatant (G) as analyzed by qRT-PCR and TCID₅₀ assay, respectively.

(H) Co-staining of MjHKU4r-CoV-1 NP (red) and hDPP4 (green) in human airway organoids at 48 h.p.i. (scale bars, 50 or 10 μ m). Blue, nuclei.

See also Figure S6.

proteases for cell entry. This has also been observed for pangolin sarbecoviruses.¹³ Moreover, a furin cleavage site was observed in MjHKU4r-CoV and MERS-CoV, but not in any of the bat HKU4r-CoVs.^{20,26} The furin cleavage site may allow MjHKU4r-CoV to replicate to high titers in the respiratory tract, as SARS-CoV-2 with the furin cleavage site deleted showed dysfunctional replication.³⁵ Notably, a genetically related pangolin HKU4r-CoV has been found in another metagenomics analysis

(HKU4/P251T/pangolin/2018, GenBank: OM009282.1), showing 98.3%, 86.3%, and 68.6% genome sequence identity to MjHKU4r-CoV-1, bat HKU4, and MERS-CoV, respectively. Importantly, the RQQR furin cleavage site was also predicted in the S protein of this HKU4r-CoV. This pangolin HKU4r-CoV was also discovered in Malayan pangolins smuggled from Southeast Asia with no information on their original inhabitant, suggesting a wide prevalence of HKU4r-CoV in pangolins.³⁶

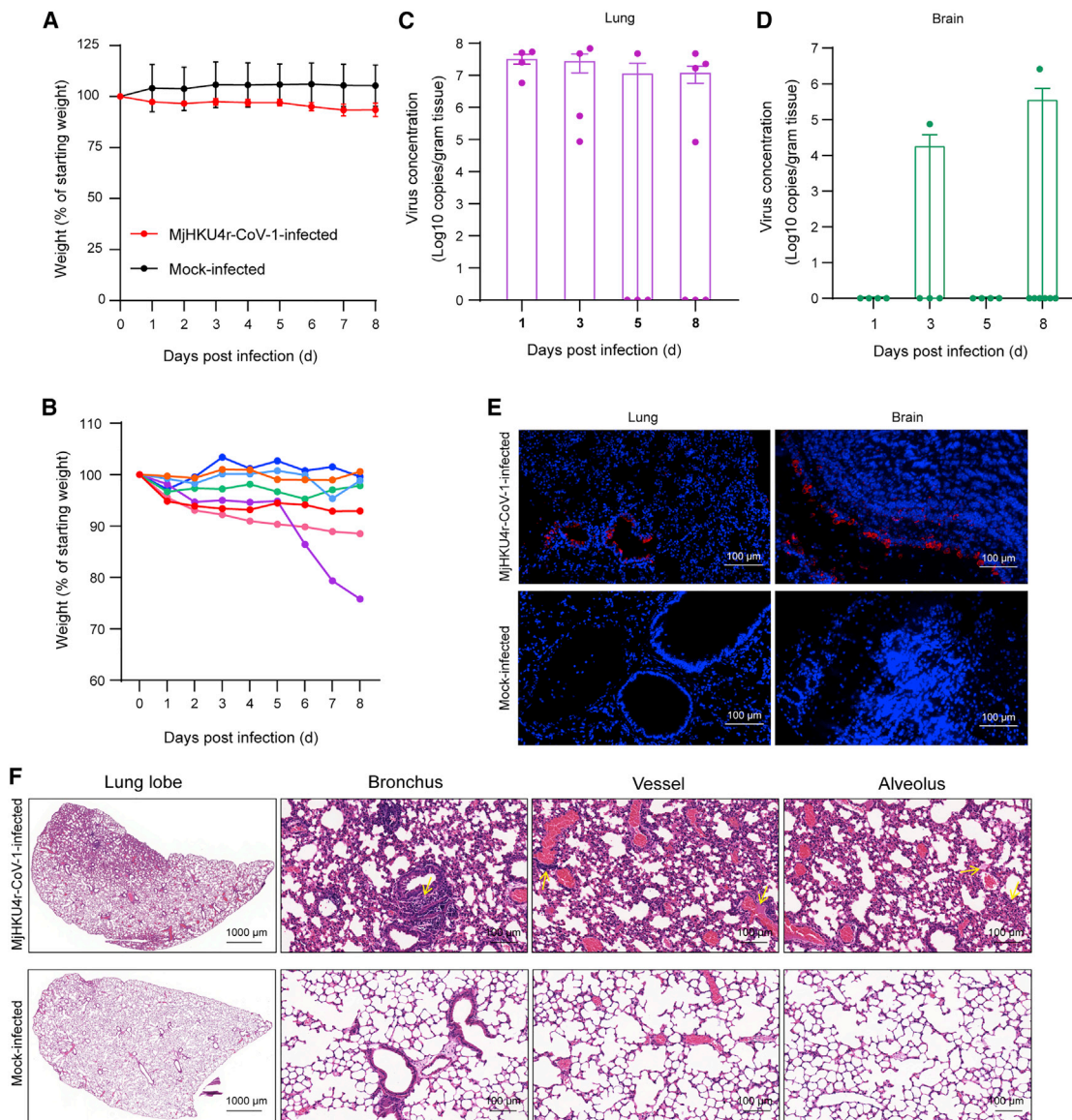


Figure 6. MjHKU4r-CoV-1 is infectious in hDPP4-Tg mice

(A and B) hDPP4-Tg mice were intranasally inoculated with 1×10^6 TCID₅₀ MjHKU4r-CoV-1. (A) Mean body weights ($n = 7$ for MjHKU4r-CoV-1 infected mice and $n = 3$ for mock-infected mice), (B) body weights of individual mice.

(C and D) qRT-PCR detection of viral replication in the lung (C) and brain (D) of MjHKU4r-CoV-1-infected hDPP4-Tg mice at the indicated time points ($n = 4$ for 1, 3, and 5 d.p.i. and $n = 7$ for 8 d.p.i.).

(E) Lung and brain sections from MjHKU4r-CoV-1-infected or mock-infected mice stained for MjHKU4r-CoV-1 NP (red) at 5 d.p.i. (lung) and 8 d.p.i. (brain) (scale bars, 100 μ m). Red, viral NP; blue, nuclei.

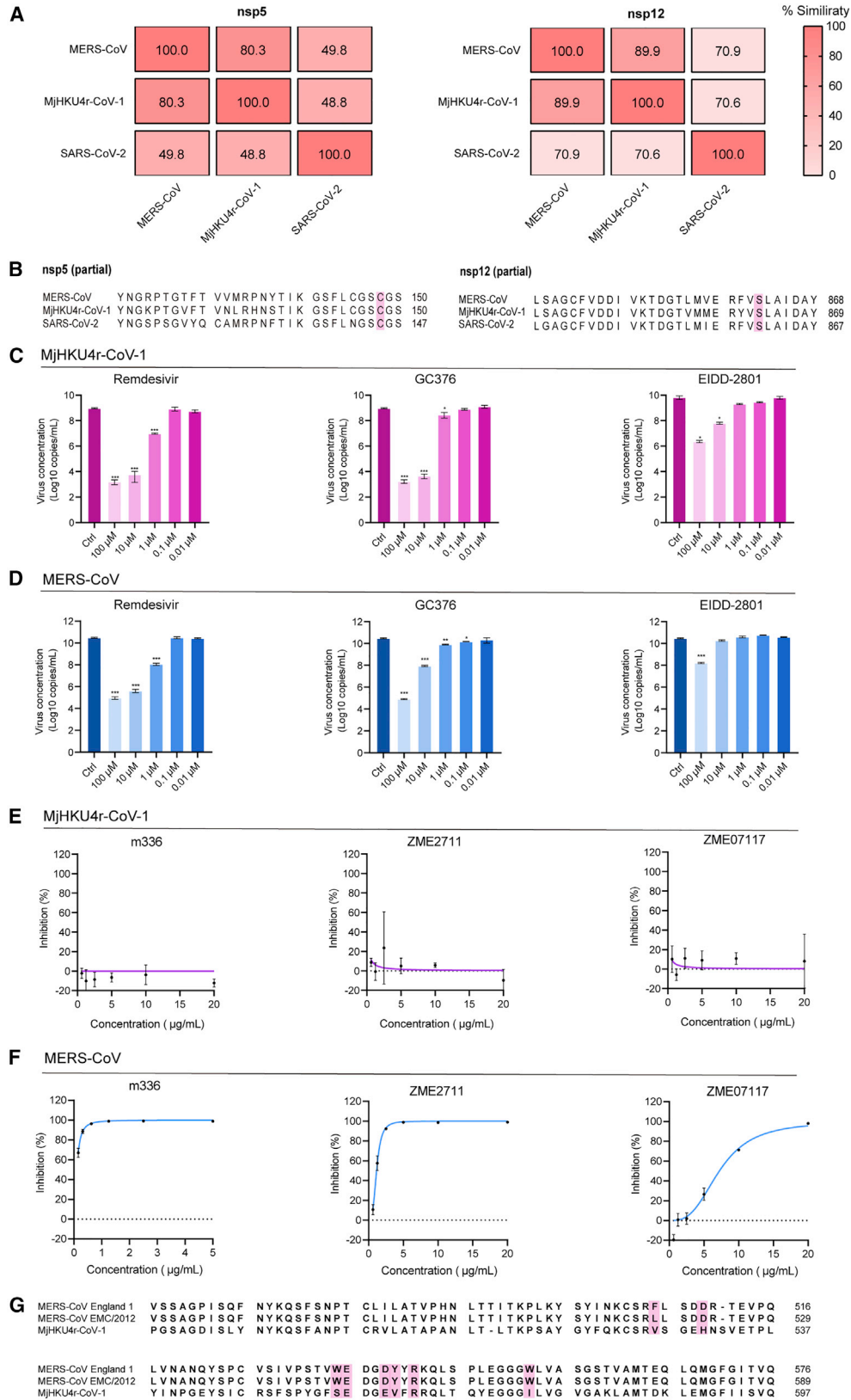
(F) Pathological changes in the lungs of MjHKU4r-CoV-1-infected hDPP4-Tg mice at 5 d.p.i. Yellow arrows indicate severely affected areas (scale bars, 1,000 or 100 μ m).

See also [Figure S7](#).

Thus, pangolins appear to be important reservoir hosts that carry bat-related, human-adapted CoVs, although the ecological relationship between pangolins and bats in the context of CoV transmission remains unclear.

The *in vitro* and *in vivo* infection experiments suggested that MjHKU4r-CoV-1 shows broad mammalian tropism and is potentially infectious and respiratory transmissible in humans,

although it may not be a highly pathogenic virus. MERS-CoV infection in hDPP4-Tg mice resulted in high lethality and severe pneumonia³⁷ in contrast to the mild to moderate lung histological injury induced by MjHKU4r-CoV-1 infection. Nevertheless, this virus may be transmitted to humans and produce efficient infection in human cells and organs. Importantly, known antibodies were not effective against this virus.



(legend on next page)

Limitations of the study

While we demonstrated that pangolins serve as a susceptible host of bat-related CoVs that are infectious in multiple human cell lines and human organoids and in a hDPP4-Tg mouse model, this study had some limitations. First, we could not determine whether the virus was spilled over directly from bats to pangolins, or whether there were any other wild animals involved. Future surveillance in bats and other game animals is needed to determine the close progenitor virus and possible transmission chain. Second, we did not perform human surveillance for any sign of spillover. As suggested by our data, the virus is potentially infectious and pathogenic to humans; therefore, we suggest active surveillance in spillover-hot occupations (e.g., animal smugglers) and areas (e.g., South East Asia). Finally, we presume that the virus is also pathogenic to pangolins. In the context of animal protection, we suggest virus detection and treatment, for example, with the small-molecule drugs used in this study, in captured pangolins.

In summary, this study demonstrated the circulation of pre-emergent MERS-like CoV related to bats in pangolins. Future surveillance is needed for a better understanding of the role of pangolins as reservoir or susceptible hosts of bat-related CoVs, and for a better preparation for the possible emergence of pangolin MERS-like CoV.

STAR★METHODS

Detailed methods are provided in the online version of this paper and include the following:

- KEY RESOURCES TABLE
- RESOURCE AVAILABILITY
 - Lead contact
 - Materials availability
 - Data and code availability
- EXPERIMENTAL MODEL AND SUBJECT DETAILS
 - hDPP4-Tg mice
- METHOD DETAILS
 - Sample collection, coronavirus identification, and sequencing
 - Serological tests
 - Virus isolation
 - High-throughput sequencing, genome alignment, and metagenomics analysis of cultured viruses
 - Phylogenetic analysis
 - Transmission electron microscopy
 - Immunofluorescence staining
 - RNA extraction and quantitative real-time PCR
 - Western blotting

- Establishment of the *hDPP4*-knockout cell line
- Construction of plasmids expressing DPP4 orthologues
- RBD and DPP4 protein expression and purification
- Biolayer interferometry
- Pseudovirus production and transduction
- Protease inhibition
- Human organoid infection, viral load determination, and IF staining
- Human tissue *ex vivo* infection, viral load determination, and IF staining
- Mouse infection
- Histological analysis
- IFN-I production and signaling luciferase reporter assays
- Antiviral assays
- Viral neutralization assessment by fluorescence reduction neutralization assay
- Biosafety and biosecurity

● QUANTIFICATION AND STATISTICAL ANALYSIS

SUPPLEMENTAL INFORMATION

Supplemental information can be found online at <https://doi.org/10.1016/j.cell.2023.01.019>.

ACKNOWLEDGMENTS

We thank Pei Zhang and Ding Gao from WIV core facility and technical support for their help with producing TEM micrographs and BLI assay. We thank Hao Tang and Jun Liu from BSL-3 Laboratory of WIV for their critical support for BSL3 facility. We thank Hui-Lan Zhang from Tongji Hospital for providing human materials. We thank Rui Gong from WIV and Jin-Cun Zhao from Guangzhou Medical University for providing mAbs, m336, ZME2711, and ZME07117. Images used in graphical abstract are adapted from BioRender. This work was jointly supported by the Strategic Priority Research Program of the Chinese Academy of Sciences (XDB29010101 to Z.-L.S. and XDB29010104 to P.Z.), China Natural Science Foundation for excellent scholars (81822028 to P.Z.), National Key R&D Program of China (2021YFC2300901 to P.Z.), Self-Supporting Program of Guangzhou Laboratory (SRPG22-001 to P.Z.), Youth Innovation Promotion Association of CAS (2019328 to X.L.Y.), National Natural Science Foundation of China (32192400), Guangxi Scientific and Technological Research (Guike AB20059002), Guangxi Medical University Training Program for Distinguished Young Scholars, and Open Research Fund Program of CAS Key Laboratory of Special Pathogens and Biosafety (2020SPCAS001).

AUTHOR CONTRIBUTIONS

Z.-L.S., P.Z., and J.C. conceived the study and prepared the manuscript. Y.H., T.Q., P.C., A.W., and M.H. collected pangolin samples. Y.T., H.S., J.L., Y.Z., B.L., D.L., B.H., J.S., and J.C. performed genome sequencing, annotations, and sequence analysis. J.C. and X.Y. performed viral isolation. W.Z. and C.W. performed protein purification and BLI assay. Y. Luo, J.C., and C.W.

Figure 7. Therapeutic treatments against MjHKU4r-CoV-1 infection

- (A) Nsp5 and nsp12 amino acid similarity between MjHKU4r-CoV-1, MERS-CoV, and SARS-CoV-2.
 (B) Partial amino acid sequence alignment of MjHKU4r-CoV-1, MERS-CoV, and SARS-CoV-2 for nsp5 and nsp12 proteins. GC376 and remdesivir target sites are shaded pink.
 (C and D) Antiviral activities of small molecules against MjHKU4r-CoV-1 (C) and MERS-CoV (D), as determined by qRT-PCR.
 (E and F) Neutralization efficacy of human monoclonal antibodies (targeting the MERS-CoV RBD) against MjHKU4r-CoV-1 (E) and MERS-CoV (F), as quantified by high content screening. Details can be found in [STAR Methods](#).
 (G) Partial S protein amino acid sequence alignment of MjHKU4r-CoV-1, MERS-CoV England 1, and MERS-CoV EMC/2012. The binding sites in RBD of MERS-CoV England 1 with m336 and the corresponding sites in MERS-CoV EMC/2012 and MjHKU4r-CoV-1 are shaded pink.
 Data are presented as means and SEMs of at least triplicate measurements in (C) and (D). Statistical significance was assessed using a two-tailed Student's t test.

established human DPP4 knockout cell lines. X.L., Q.G., X.Y., S.X., and R.J. helped with or performed the organoids culturing and IF staining. J.C., H.L., T.J., R.J., and Y.C. performed animal experiments and histology analysis. J.C. and Y. Li performed main experiment and Q.L., M.L., X.Z., A.L., Y. Yao, and Y. Yang provided help. All authors reviewed and edited the paper.

DECLARATION OF INTERESTS

The authors declare no competing interests.

Received: June 2, 2022

Revised: November 17, 2022

Accepted: January 12, 2023

Published: February 16, 2023

REFERENCES

- Cui, J., Li, F., and Shi, Z.-L. (2019). Origin and evolution of pathogenic coronaviruses. *Nat. Rev. Microbiol.* *17*, 181–192. <https://doi.org/10.1038/s41579-018-0118-9>.
- Zhou, P., Yang, X.-L., Wang, X.-G., Hu, B., Zhang, L., Zhang, W., Si, H.-R., Zhu, Y., Li, B., Huang, C.-L., et al. (2020). A pneumonia outbreak associated with a new coronavirus of probable bat origin. *Nature* *579*, 270–273. <https://doi.org/10.1038/s41586-020-2012-7>.
- Hu, B., Zeng, L.-P., Yang, X.-L., Ge, X.-Y., Zhang, W., Li, B., Xie, J.-Z., Shen, X.-R., Zhang, Y.-Z., Wang, N., et al. (2017). Discovery of a rich gene pool of bat SARS-related coronaviruses provides new insights into the origin of SARS coronavirus. *PLOS Pathog.* *13*, e1006698. <https://doi.org/10.1371/journal.ppat.1006698>.
- Zaki, A.M., van Boheemen, S., Bestebroer, T.M., Osterhaus, A.D.M.E., and Fouchier, R.A.M. (2012). Isolation of a novel coronavirus from a man with pneumonia in Saudi Arabia. *N. Engl. J. Med.* *367*, 1814–1820. <https://doi.org/10.1056/NEJMoa1211721>.
- Zhao, K., Zhang, W., Li, B., Xie, S.-Z., Yi, F., Jiang, R.-D., Luo, Y., He, X.-Y., Zhang, Y.-Z., Shi, Z.-L., et al. (2022). Ecological study of cave nectar bats reveals low risk of direct transmission of bat viruses to humans. *Zool. Res.* *43*, 514–522. <https://doi.org/10.24272/j.issn.2095-8137.2021.480>.
- Chinese SARS Molecular Epidemiology Consortium (2004). Molecular evolution of the SARS coronavirus during the course of the SARS epidemic in China. *Science* *303*, 1666–1669. <https://doi.org/10.1126/science.1092002>.
- Li, W., Zhang, C., Sui, J., Kuhn, J.H., Moore, M.J., Luo, S., Wong, S.-K., Huang, I.-C., Xu, K., Vasilieva, N., et al. (2005). Receptor and viral determinants of SARS-coronavirus adaptation to human ACE2. *EMBO J.* *24*, 1634–1643. <https://doi.org/10.1038/sj.emboj.7600640>.
- Song, H.-D., Tu, C.-C., Zhang, G.-W., Wang, S.-Y., Zheng, K., Lei, L.-C., Chen, Q.-X., Gao, Y.-W., Zhou, H.-Q., Xiang, H., et al. (2005). Cross-host evolution of severe acute respiratory syndrome coronavirus in palm civet and human. *Proc. Natl. Acad. Sci. USA* *102*, 2430–2435. <https://doi.org/10.1073/pnas.0409608102>.
- Ge, X.-Y., Li, J.-L., Yang, X.-L., Chmura, A.A., Zhu, G., Epstein, J.H., Mazet, J.K., Hu, B., Zhang, W., Peng, C., et al. (2013). Isolation and characterization of a bat SARS-like coronavirus that uses the ACE2 receptor. *Nature* *503*, 535–538. <https://doi.org/10.1038/nature12711>.
- Yang, X.-L., Hu, B., Wang, B., Wang, M.-N., Zhang, Q., Zhang, W., Wu, L.-J., Ge, X.-Y., Zhang, Y.-Z., Daszak, P., et al. (2015). Isolation and characterization of a novel bat coronavirus closely related to the direct progenitor of severe acute respiratory syndrome coronavirus. *J. Virol.* *90*, 3253–3256. <https://doi.org/10.1128/JVI.02582-15>.
- Lam, T.-T., Jia, N., Zhang, Y.-W., Shum, M.H.-H., Jiang, J.-F., Zhu, H.-C., Tong, Y.-G., Shi, Y.-X., Ni, X.-B., Liao, Y.-S., et al. (2020). Identifying SARS-CoV-2-related coronaviruses in Malayan pangolins. *Nature* *583*, 282–285. <https://doi.org/10.1038/s41586-020-2169-0>.
- Xiao, K., Zhai, J., Feng, Y., Zhou, N., Zhang, X., Zou, J.-J., Li, N., Guo, Y., Li, X., Shen, X., et al. (2020). Isolation of SARS-CoV-2-related coronavirus from Malayan pangolins. *Nature* *583*, 286–289. <https://doi.org/10.1038/s41586-020-2313-x>.
- Zhang, S., Qiao, S., Yu, J., Zeng, J., Shan, S., Tian, L., Lan, J., Zhang, L., and Wang, X. (2021). Bat and pangolin coronavirus spike glycoprotein structures provide insights into SARS-CoV-2 evolution. *Nat. Commun.* *12*, 1607. <https://doi.org/10.1038/s41467-021-21767-3>.
- Fan, H.-H., Wang, L.-Q., Liu, W.-L., An, X.-P., Liu, Z.-D., He, X.-Q., Song, L.-H., and Tong, Y.-G. (2020). Repurposing of clinically approved drugs for treatment of coronavirus disease 2019 in a 2019-novel coronavirus-related coronavirus model. *Chin. Med. J. (Engl)* *133*, 1051–1056. <https://doi.org/10.1097/CM9.0000000000000797>.
- Peng, M.-S., Li, J.-B., Cai, Z.-F., Liu, H., Tang, X., Ying, R., Zhang, J.-N., Tao, J.-J., Yin, T.-T., Zhang, T., et al. (2021). The high diversity of SARS-CoV-2-related coronaviruses in pangolins alerts potential ecological risks. *Zool. Res.* *42*, 834–844. <https://doi.org/10.24272/j.issn.2095-8137.2021.334>.
- Wacharapluesadee, S., Tan, C.W., Maneerorn, P., Duengkae, P., Zhu, F., Joyjinda, Y., Kaewpom, T., Chia, W.N., Ampoot, W., Lim, B.L., et al. (2021). Evidence for SARS-CoV-2 related coronaviruses circulating in bats and pangolins in Southeast Asia. *Nat. Commun.* *12*, 972. <https://doi.org/10.1038/s41467-021-21240-1>.
- Liu, P., Chen, W., and Chen, J.P. (2019). Viral metagenomics revealed Sendai virus and coronavirus infection of Malayan pangolins (*Manis javanica*). *Viruses* *11*. <https://doi.org/10.3390/v11110979>.
- ICTV. International Committee on Taxonomy of Viruses. <http://ictv.global/taxonomy>.
- Burbelo, P.D., Hoshino, Y., Leahy, H., Krogmann, T., Hornung, R.L., Iadarola, M.J., and Cohen, J.I. (2009). Serological diagnosis of human herpes simplex virus type 1 and 2 infections by luciferase immunoprecipitation system assay. *Clin. Vaccine Immunol.* *16*, 366–371. <https://doi.org/10.1128/CVI.00350-08>.
- Millet, J.K., and Whittaker, G.R. (2014). Host cell entry of Middle East respiratory syndrome coronavirus after two-step, furin-mediated activation of the spike protein. *Proc. Natl. Acad. Sci. USA* *111*, 15214–15219. <https://doi.org/10.1073/pnas.1407087111>.
- Lu, G., Wang, Q., and Gao, G.F. (2015). Bat-to-human: spike features determining ‘host jump’ of coronaviruses SARS-CoV, MERS-CoV, and beyond. *Trends Microbiol.* *23*, 468–478. <https://doi.org/10.1016/j.tim.2015.06.003>.
- Wang, Q., Qi, J., Yuan, Y., Xuan, Y., Han, P., Wan, Y., Ji, W., Li, Y., Wu, Y., Wang, J., et al. (2014). Bat origins of MERS-CoV supported by bat coronavirus HKU4 usage of human receptor CD26. *Cell Host Microbe* *16*, 328–337. <https://doi.org/10.1016/j.chom.2014.08.009>.
- Lau, S.K.P., Fan, R.Y.Y., Zhu, L., Li, K.S.M., Wong, A.C.P., Luk, H.K.H., Wong, E.Y.M., Lam, C.S.F., Lo, G.C.S., Fung, J., et al. (2021). Isolation of MERS-related coronavirus from lesser bamboo bats that uses DPP4 and infects human-DPP4-transgenic mice. *Nat. Commun.* *12*, 216. <https://doi.org/10.1038/s41467-020-20458-9>.
- Johnson, B.A., Xie, X., Bailey, A.L., Kalveram, B., Lokugamage, K.G., Muruato, A., Zou, J., Zhang, X., Juelich, T., Smith, J.K., et al. (2021). Loss of furin cleavage site attenuates SARS-CoV-2 pathogenesis. *Nature* *591*, 293–299. <https://doi.org/10.1038/s41586-021-03237-4>.
- Menachery, V.D., Dinnon 3rd, K.H.D., Yount, B.L., McAnarney, E.T., Gralinski, L.E., Hale, A., Graham, R.L., Scobey, T., Anthony, S.J., Wang, L., et al. (2020). Trypsin treatment unlocks barrier for zoonotic bat coronavirus infection. *J. Virol.* *94*. <https://doi.org/10.1128/JVI.01774-19>.
- Yang, Y., Du, L., Liu, C., Wang, L., Ma, C., Tang, J., Baric, R.S., Jiang, S., and Li, F. (2014). Receptor usage and cell entry of bat coronavirus HKU4 provide insight into bat-to-human transmission of MERS coronavirus. *Proc. Natl. Acad. Sci. USA* *111*, 12516–12521. <https://doi.org/10.1073/pnas.1405889111>.

27. Park, J.E., Li, K., Barlan, A., Fehr, A.R., Perlman, S., McCray, P.B., Jr., and Gallagher, T. (2016). Proteolytic processing of Middle East respiratory syndrome coronavirus spikes expands virus tropism. *Proc. Natl. Acad. Sci. USA* *113*, 12262–12267. <https://doi.org/10.1073/pnas.1608147113>.
28. Channappanavar, R., and Perlman, S. (2017). Pathogenic human coronavirus infections: causes and consequences of cytokine storm and immunopathology. *Semin. Immunopathol.* *39*, 529–539. <https://doi.org/10.1007/s00281-017-0629-x>.
29. Sheahan, T.P., Sims, A.C., Graham, R.L., Menachery, V.D., Gralinski, L.E., Case, J.B., Leist, S.R., Pirc, K., Feng, J.Y., Trantcheva, I., et al. (2017). Broad-spectrum antiviral GS-5734 inhibits both epidemic and zoonotic coronaviruses. *Sci. Transl. Med.* *9*, eaa13653. <https://doi.org/10.1126/scitranslmed.aal3653>.
30. Sheahan, T.P., Sims, A.C., Zhou, S., Graham, R.L., Pruijssers, A.J., Agostini, M.L., Leist, S.R., Schäfer, A., Dinno, K.H., 3rd, Stevens, L.J., et al. (2020). An orally bioavailable broad-spectrum antiviral inhibits SARS-CoV-2 in human airway epithelial cell cultures and multiple coronaviruses in mice. *Sci. Transl. Med.* *12*, eabb5883. <https://doi.org/10.1126/scitranslmed.abb5883>.
31. Rathnayake, A.D., Zheng, J., Kim, Y., Perera, K.D., Mackin, S., Meyerholz, D.K., Kashipathy, M.M., Battaile, K.P., Lovell, S., Perlman, S., et al. (2020). 3C-like protease inhibitors block coronavirus replication in vitro and improve survival in MERS-CoV-infected mice. *Sci. Transl. Med.* *12*, eabc5332. <https://doi.org/10.1126/scitranslmed.abc5332>.
32. Ying, T., Du, L., Ju, T.W., Prabaharan, P., Lau, C.C., Lu, L., Liu, Q., Wang, L., Feng, Y., Wang, Y., et al. (2014). Exceptionally potent neutralization of Middle East respiratory syndrome coronavirus by human monoclonal antibodies. *J. Virol.* *88*, 7796–7805. <https://doi.org/10.1128/JVI.00912-14>.
33. Vora, N.M., Hannah, L., Lieberman, S., Vale, M.M., Plowright, R.K., and Bernstein, A.S. (2022). Want to prevent pandemics? Stop spillovers. *Nature* *605*, 419–422. <https://doi.org/10.1038/d41586-022-01312-y>.
34. Yang, Y., Liu, C., Du, L., Jiang, S., Shi, Z., Baric, R.S., and Li, F. (2015). Two mutations were critical for bat-to-human transmission of Middle East respiratory syndrome coronavirus. *J. Virol.* *89*, 9119–9123. <https://doi.org/10.1128/JVI.01279-15>.
35. Peacock, T.P., Goldhill, D.H., Zhou, J., Baillon, L., Frise, R., Swann, O.C., Kugathasan, R., Penn, R., Brown, J.C., Sanchez-David, R.Y., et al. (2021). The furin cleavage site in the SARS-CoV-2 spike protein is required for transmission in ferrets. *Nat. Microbiol.* *6*, 899–909. <https://doi.org/10.1038/s41564-021-00908-w>.
36. Shi, W., Shi, M., Que, T.-C., Cui, X.-M., Ye, R.-Z., Xia, L.-Y., Hou, X., Zheng, J.-J., Jia, N., Xie, X., et al. (2022). Trafficked Malayan pangolins contain viral pathogens of humans. *Nat. Microbiol.* *7*, 1259–1269. <https://doi.org/10.1038/s41564-022-01181-1>.
37. Agrawal, A.S., Garron, T., Tao, X., Peng, B.-H., Wakamiya, M., Chan, T.-S., Couch, R.B., and Tseng, C.-T.K. (2015). Generation of a transgenic mouse model of Middle East respiratory syndrome coronavirus infection and disease. *J. Virol.* *89*, 3659–3670. <https://doi.org/10.1128/JVI.03427-14>.
38. Chen, J., Hu, B.J., Zhao, K., Luo, Y., Lin, H.F., and Shi, Z.L. (2021). Development of a MERS-CoV replicon cell line for antiviral screening. *Virology* *500*, 730–735. <https://doi.org/10.1007/s12250-020-00341-z>.
39. Guo, H., Hu, B., Si, H.-R., Zhu, Y., Zhang, W., Li, B., Li, A., Geng, R., Lin, H.-F., Yang, X.-L., et al. (2021). Identification of a novel lineage bat SARS-related coronaviruses that use bat ACE2 receptor. *Emerg. Microbes Infect.* *10*, 1507–1514. <https://doi.org/10.1080/22221751.2021.1956373>.
40. Latinné, A., Hu, B., Olival, K.J., Zhu, G., Zhang, L., Li, H., Chmura, A.A., Field, H.E., Zambrana-Torrel, C., Epstein, J.H., et al. (2020). Origin and cross-species transmission of bat coronaviruses in China. *Nat. Commun.* *11*, 4235. <https://doi.org/10.1038/s41467-020-17687-3>.
41. Martin, M. (2011). Cutadapt removes adapter sequences from high-throughput sequencing reads. *EMBnet.journal* *17*, 10–12. <https://doi.org/10.14806/ej.17.1.200>.
42. Li, D., Liu, C.M., Luo, R., Sadakane, K., and Lam, T.W. (2015). MEGAHIT: an ultra-fast single-node solution for large and complex metagenomics assembly via succinct de Bruijn graph. *Bioinformatics Oxf. Engl.* *31*, 1674–1676. <https://doi.org/10.1093/bioinformatics/btv033>.
43. Petersen, T.N., Lukjancenko, O., Thomsen, M.C.F., Maddalena Sperotto, M., Lund, O., Møller Aarestrup, F., and Sicheritz-Pontén, T. (2017). MGMapper: reference based mapping and taxonomy annotation of metagenomics sequence reads. *PLoS One* *12*, e0176469. <https://doi.org/10.1371/journal.pone.0176469>.
44. Li, H., and Durbin, R. (2010). Fast and accurate long-read alignment with Burrows-Wheeler transform. *Bioinformatics* *26*, 589–595. <https://doi.org/10.1093/bioinformatics/btp698>.
45. Nguyen, L.T., Schmidt, H.A., von Haeseler, A., and Minh, B.Q. (2015). IQ-TREE: a fast and effective stochastic algorithm for estimating maximum-likelihood phylogenies. *Mol. Biol. Evol.* *32*, 268–274. <https://doi.org/10.1093/molbev/msu300>.
46. Katoh, K., Misawa, K., Kuma, K., and Miyata, T. (2002). MAFFT: a novel method for rapid multiple sequence alignment based on fast Fourier transform. *Nucleic Acids Res.* *30*, 3059–3066. <https://doi.org/10.1093/nar/gkf436>.
47. Kumar, S., Stecher, G., and Tamura, K. (2016). MEGA7: molecular evolutionary genetics analysis version 7.0 for bigger datasets. *Mol. Biol. Evol.* *33*, 1870–1874. version 7.0. <https://doi.org/10.1093/molbev/msw054>.
48. Lole, K.S., Bollinger, R.C., Paranjape, R.S., Gadkari, D., Kulkarni, S.S., Novak, N.G., Ingersoll, R., Sheppard, H.W., and Ray, S.C. (1999). Full-length human immunodeficiency virus type 1 genomes from subtype C-infected seroconverters in India, with evidence of intersubtype recombination. *J. Virol.* *73*, 152–160. <https://doi.org/10.1128/JVI.73.1.152-160.1999>.
49. Schindelin, J., Rueden, C.T., Hiner, M.C., and Eliceiri, K.W. (2015). The ImageJ ecosystem: an open platform for biomedical image analysis. *Mol. Reprod. Dev.* *82*, 518–529. <https://doi.org/10.1002/mrd.22489>.
50. Yuan, Y., Cao, D., Zhang, Y., Ma, J., Qi, J., Wang, Q., Lu, G., Wu, Y., Yan, J., Shi, Y., et al. (2017). Cryo-EM structures of MERS-CoV and SARS-CoV spike glycoproteins reveal the dynamic receptor binding domains. *Nat. Commun.* *8*, 15092. <https://doi.org/10.1038/ncomms15092>.
51. Zhou, P., Fan, H., Lan, T., Yang, X.L., Shi, W.F., Zhang, W., Zhu, Y., Zhang, Y.W., Xie, Q.M., Mani, S., et al. (2018). Fatal swine acute diarrhoea syndrome caused by an HKU2-related coronavirus of bat origin. *Nature* *556*, 255–258. <https://doi.org/10.1038/s41586-018-0010-9>.
52. Li, Q., Wu, J., Nie, J., Zhang, L., Hao, H., Liu, S., Zhao, C., Zhang, Q., Liu, H., Nie, L., et al. (2020). The impact of mutations in SARS-CoV-2 spike on viral infectivity and antigenicity. *Cell* *182*, 1284–1294.e9. <https://doi.org/10.1016/j.cell.2020.07.012>.
53. Sachs, N., Pappaspyropoulos, A., Zomer-van Ommen, D.D., Heo, I., Böttinger, L., Klay, D., Weeber, F., Huelsz-Prince, G., Jakobachvili, N., Amantgalim, G.D., et al. (2019). Long-term expanding human airway organoids for disease modeling. *EMBO J.* *38*, e100300. <https://doi.org/10.15252/embj.2018100300>.
54. Sato, T., Stange, D.E., Ferrante, M., Vries, R.G., Van Es, J.H., Van den Brink, S., Van Houdt, W.J., Pronk, A., Van Gorp, J., Siersema, P.D., and Clevers, H. (2011). Long-term expansion of epithelial organoids from human colon, adenoma, adenocarcinoma, and Barrett's epithelium. *Gastroenterology* *141*, 1762–1772. <https://doi.org/10.1053/j.gastro.2011.07.050>.

STAR★METHODS

KEY RESOURCES TABLE

REAGENT or RESOURCE	SOURCE	IDENTIFIER
Antibodies		
Goat Anti-Rabbit IgG H&L (Cy3) preadsorbed	Abcam	Cat#: ab6939; RRID:AB_955021
Goat Anti-Mouse IgG H&L (Alexa Fluor 488) preadsorbed	Abcam	Cat#: ab150117; RRID:AB_2688012
DYKDDDDK-Tag(3B9) mAb (Same as Sigma's Anti-FLAG M2)	Abmart	Cat#:M20008L; RRID:AB_2713960
Anti-VSV-G [8G5F11] Antibody	Kerafast	Cat#: EB0010; RRID:AB_2811223
Anti-VSV-M [23H12] Antibody	Kerafast	Cat#: EB0011; RRID:AB_2734773
GAPDH Monoclonal antibody	Proteintech	Cat#:60004-1-Ig; RRID:AB_2107436
HRP-conjugated Affinipure Goat Anti-Mouse IgG(H+L)	Proteintech	Cat#:SA00001-1; RRID:AB_2722565
Human DPP4/CD26 Antibody	R&D systems	Cat#: AF1180; RRID:AB_354651
Donkey Anti-Goat IgG H&L (Alexa Fluor 488)	Abcam	Cat#: ab150129; RRID:AB_2687506
Cy3 AffiniPure Donkey Anti-Rabbit IgG (H+L)	Jackson Lab	Cat#: 711-165-152; RRID:AB_2307443
Rabbit anti-Tylonycteris bat coronavirus HKU4 N protein polyclonal antibody	This paper	N/A
Rabbit anti-MERS-CoV EMC/2012 N protein polyclonal antibody	Chen et al. ³⁸	N/A
Mouse anti-S tag monoclonal antibody	Zhou et al. ²	N/A
m336	Ying et al. ³²	N/A
ZME2711	This paper	N/A
ZME07117	This paper	N/A
Bacterial and virus strains		
MjHKU4r-CoV-1	Isolated from pangolin anal swab sample	N/A
MERS-CoV	Rescue by reverse genetics	N/A
VSV*ΔG-FLuc	Guo et al. ³⁹	N/A
ElectroMAX™ DH10B T1 Phage-Resistant Competent Cells	Thermo Fisher Scientific	Cat#: 12033015
Biological samples		
Pangolin anal swab and serum sample	This paper	N/A
Chemicals, peptides, and recombinant proteins		
Lipofectamine 3000	Thermo Fisher Scientific	Cat#: L3000015
DAPI	Beyotime	Cat#: C1002
tribromoethanol (Avertin)	Sigma	Cat#: T-48402
4% paraformaldehyde	Boster	Cat#: AR1068
RNAlater Stabilization Solution	Invitrogen	Cat#: AM7021
Furin inhibitor, decanoyl-RVKR-CMK	Tocris	Cat#: 3501
Camostat	MedChemExpress	Cat#: HY-13512
E64D	Selleck	Cat#: S7393
Remdesivir	Selleck	Cat#: S8932
GC376	Selleck	Cat#: S0475
EIDD-2801	Selleck	Cat#: S8969
MjHKU4r-CoV-1 RBD	This paper	N/A
MERS-CoV RBD	This paper	N/A
HKU4 RBD	This paper	N/A
hDPP4	This paper	N/A

(Continued on next page)

Continued

REAGENT or RESOURCE	SOURCE	IDENTIFIER
TpDPP4	This paper	N/A
PpDPP4	This paper	N/A
MjDPP4	This paper	N/A
EZ-Link NHS-LC-LC-Biotin	Thermo Fisher Scientific	Cat#: 29986
Universal Type I IFN Protein	R&D systems	Cat#: 11200-1
TRIzol Reagent	Invitrogen	Cat#: 15596026
Protein A/G UltraLink Resin	Thermo Fisher Scientific	Cat#: 53132
Matrigel	CORNING	Cat#: 356231

Critical commercial assays

HiSxript II One step qRT-PCR SYBR Green Kit	Vazyme	Cat#: Q221-01
Bright-Lite Luciferase Assay System	Vazyme	Cat#: DD1204
Dual-Luciferase Reporter Assay System	Promega	Cat#: E1960
QIAamp 96 Virus QIAcube HT Kit	QIAGEN	Cat#: 57731
QIAamp Viral RNA Mini Kit	Qiagen	Cat#: 52906
Virus DNA/RNA Extraction Kit	Vazyme	Cat#: RM401-04
SMARTER RACE 5'/3' Kit	Takara	Cat#: 634858
SuperScript III One-Step RT-PCR System with Platinum Taq	Thermo Fisher Scientific	Cat#: 12574026
RNAprep Pure Cell/Bacteria Kit	TIANGEN	Cat#: DP430
HiScript II 1st Strand cDNA Synthesis Kit	Vazyme	Cat#: R211
Taq Pro Universal SYBR qPCR Master Mix	Vazyme	Cat#: Q712
Renilla Luciferase Assay System	Promega	Cat#: E2820
MGEasy RNA Library Prep Set	MGI	Cat#: 1000006384
MGISEQ-2000RS High-throughput Fast Sequencing Reagent Kit (FCL PE150)	MGI	Cat#: 1000012555

Deposited data

Raw sequencing reads	This paper	NGDC-GSA: CRA006906
Viral genomes data	This paper	NGDC-GWH: GWHBHAL01000000, GWHBIUK01000000, GWHBIUL01000000, GWHBIUM01000000
Phylogenetic tree data	This paper	https://doi.org/10.6084/m9.figshare.21679361.v1

Experimental models: Cell lines

HEK293	Laboratory of Linfa Wang	ATCC Cat#: CRL-1573; RRID: CVCL_0045
A549	ATCC	ATCC Cat#: CCL-185
Calu-3	ATCC	ATCC Cat#: HTB-55; RRID: CVCL_0609
Huh-7	Laboratory of Xinwen Chen	RRID: CVCL_0336
Caco-2	ATCC	ATCC Cat#: HTB-37; RRID: CVCL_0025
HeLa	Laboratory of Linfa Wang	ATCC Cat#: CRM-CCL-2; RRID: CVCL_0030
HEp-2	ATCC	ATCC Cat#: CCL-23; RRID: CVCL_1906
hDPP4 knock-out Huh-7	This paper	N/A

Experimental models: Organisms/strains

Mouse: C57BL/6 human DPP4 transgenic mouse (hDPP4-Tg)	This paper	N/A
---	------------	-----

Oligonucleotides

F-MjHKU4r-CoV-1-ORF5 CTTCGTGTTGATAAT GGTACTTCC	This paper	N/A
R-MjHKU4r-CoV-1-ORF5 AGCAGAGTGACATAGAAACA	This paper	N/A

(Continued on next page)

Continued

REAGENT or RESOURCE	SOURCE	IDENTIFIER
F-MERS-CoV-NP GGGTGTACCTCTTAATGCCAATTC	Chen et al. ³⁸	N/A
MERS-CoV-NP TCTGTCCTGTCTCCGCCAAT	Chen et al. ³⁸	N/A
human IFN β CTTGGATTCTACAAAGAAGCAGC	This paper	N/A
R-human IFN β TCCTCCTTCTGGAAGTCTGCA	This paper	N/A
F-human ISG15 CTCTGAGCATCCTGGTGAGGAA	This paper	N/A
R-human ISG15 AAGTTCAGCCAGAACAGGTCGT	This paper	N/A
F-human GAPDH ACAACCTTTGGTATCGTGGAAGG	This paper	N/A
R-human GAPDH GCCATCACGCCACAGTTTC	This paper	N/A
CoV-FWD3: GGTTGGGAYTAYCCHAARTGTGA	Latinne et al. ⁴⁰	N/A
CoV-RVS3: CCATCATCASWYRAATCATCATA	Latinne et al. ⁴⁰	N/A
CoV-FWD4/Other: GAYTAYCCHAARTGTGA UMGWGC)	Latinne et al. ⁴⁰	N/A

Recombinant DNA

Plasmid: pcDNA3.1-MERS-S-Stag	This paper	N/A
Plasmid: pcDNA3.1-MjHKU4r-CoV-1 WT-S-Stag	This paper	N/A
Plasmid: pcDNA3.1-MjHKU4r-CoV-1- Mut-S-Stag	This paper	N/A
Plasmid: pcDNA3.1-HKU4-CoV-S-Stag	This paper	N/A
Plasmid: pCMV-3Tag-8-Human furin	This paper	N/A
Plasmid: pCMV-3Tag-8-Human DPP4	This paper	N/A
Plasmid: pCMV-3Tag-8-TpDPP4	This paper	N/A
Plasmid: pCMV-3Tag-8-PpDPP4	This paper	N/A
Plasmid: pCMV-3Tag-8-MjDPP4	This paper	N/A
Plasmid: pCMV-3Tag-8-mouse DPP4	This paper	N/A
Plasmid: pCMV-3Tag-8-ferret DPP4	This paper	N/A
Plasmid: pCMV-3Tag-8-pig DPP4	This paper	N/A
Plasmid: pCMV-3Tag-8-goat DPP4	This paper	N/A
Plasmid: pCMV-3Tag-8-cat DPP4	This paper	N/A
Plasmid: pCMV-3Tag-8-rabbit DPP4	This paper	N/A
Plasmid: pCMV-3Tag-8-horse DPP4	This paper	N/A
Plasmid: pCMV-3Tag-8-rat DPP4	This paper	N/A
Plasmid: pCMV-3Tag-8-macaque DPP4	This paper	N/A
Plasmid: pCMV-3Tag-8-sheep DPP4	This paper	N/A
Plasmid: pCMV-3Tag-8-hamster DPP4	This paper	N/A
Plasmid: pCMV-3Tag-8-camel DPP4	This paper	N/A
Plasmid: pCMV-3Tag-8-marmoset DPP4	This paper	N/A
Plasmid: pCMV-3Tag-8-cattle DPP4	This paper	N/A
Plasmid: pCMV-3Tag-8-dog DPP4	This paper	N/A
Plasmid: pCMV-3Tag-8-S	This paper	N/A
Plasmid: pCMV-3Tag-8-E	This paper	N/A
Plasmid: pCMV-3Tag-8-M	This paper	N/A

(Continued on next page)

Continued

REAGENT or RESOURCE	SOURCE	IDENTIFIER
Plasmid: pCMV-3Tag-8-N	This paper	N/A
Plasmid: pCMV-3Tag-8-ORF3	This paper	N/A
Plasmid: pCMV-3Tag-8-ORF4a	This paper	N/A
Plasmid: pCMV-3Tag-8-ORF4b	This paper	N/A
Plasmid: pCMV-3Tag-8-ORF5	This paper	N/A
Plasmid: pCMV-3Tag-8-ORF8b	This paper	N/A
Plasmid: pREN2-MjHKU4r-CoV-1 N	This paper	N/A

Software and algorithms

Cutadapt (v1.18)	Kechin et al. ⁴¹	https://cutadapt.readthedocs.io/en/stable/index.html
Geneious (v11.0.3)	Dotmatics	https://www.geneious.com/
Megahit (v1.2.9)	Li et al. ⁴²	https://github.com/voutcn/megahit
MGMapper (PE_2.24 and SE_2.24)	Petersen et al. ⁴³	https://bitbucket.org/genomicepidemiology/mgmapper/src/master/
BWA (v0.7.12-r1039)	Li et al. ⁴⁴	https://github.com/lh3/bwa
BioEdit (v7.1.3.0)	software.informer	http://www.mbio.ncsu.edu/BioEdit/bioedit.html
figtree (v1.4.3)	Andrew Rambaut	http://tree.bio.ed.ac.uk/software/Figtree/
IQ-TREE (v1.6.1)	Barbetti et al. ⁴⁵	http://www.iqtree.org/about/
mafft (v7.407)	Katoh et al. ⁴⁶	https://mafft.cbrc.jp/alignment/software/
Mega (v7.0.18)	Kumar et al. ⁴⁷	https://megasoftware.net/
SimPlot (v3.5.1)	Lole et al. ⁴⁸	https://sray.med.som.jhmi.edu/SCRoftware/SimPlot/
ImageJ	Schindelin et al. ⁴⁹	https://imagej.nih.gov/ij/
GraphPad Prism (version 8.0.2(263))	GraphPad Software	https://www.graphpad.com/

Other

Prefusion structure of MERS-CoV spike glycoprotein	Yuan et al. ⁵⁰	https://www.rcsb.org/structure/5X5C
--	---------------------------	---

RESOURCE AVAILABILITY

Lead contact

Further information and requests for resources and reagents should be directed to and will be fulfilled by the lead contact, Peng Zhou (peng.zhou@wh.iov.cn or zhou_peng@gzlab.ac.cn).

Materials availability

The materials used and generated in this study are available from the **lead contact** upon reasonable request with a completed Material Transfer Agreement.

Data and code availability

- The NGS raw data of MjHKU4r-CoV-1, MjHKU4r-CoV-2, MjHKU4r-CoV-3 and MjHKU4r-CoV-4 sequences have been submitted to GSA (Genome Sequence Archive) with accession number: CRA006906.
- The full-length genome sequences of MjHKU4r-CoV-1, MjHKU4r-CoV-2, MjHKU4r-CoV-3 and MjHKU4r-CoV-4 have been deposited into NGDC (National Genomics Data Center) database and the original code are listed in the **key resources table**.
- Any additional information required to reanalyze the data reported in this paper is available from the **Lead Contact** upon request.

EXPERIMENTAL MODEL AND SUBJECT DETAILS

hDPP4-Tg mice

The hDPP4-Tg mouse model was established at Cyagen company following the protocol described by Anurodh et al.³⁷ The transgene cassette expressing hDPP4 was constructed using the pCAGGS plasmid. Tg mice with global hDPP4 overexpression were

generated by microinjection of C57BL/6 × C57BL/6 zygotes with an expression cassette consisting of the CAG promoter elements and the coding region of the *hDPP4* gene. Founder mice were identified and crossed with C57BL/6 mice, and all pups of each founder were tested for hDPP4 expression by PCR. hDPP4 expression in different tissues of hDPP4-Tg mice was determined by quantitative PCR and western blotting. Twelve male and thirteen female mice at seven to fourteen weeks-old were used in this study. Littermates of the same sex were randomly assigned to mock, 1, 3, 5 d.p.i. and survival groups. All *in vivo* infection experiments were conducted in a biosafety level 3 (BSL3) laboratory in accordance with the recommendations for the care and use of laboratory animals and under the approval of the Institute Review Board of Wuhan Institute of Virology, Chinese Academy of Sciences (approval number WIVAF05202201).

METHOD DETAILS

Sample collection, coronavirus identification, and sequencing

During 2019 and 2020, 86 anal swab samples and 80 serum samples (bleeding was not successful for six animals) were collected from pangolins according to the animal ethics permit issued by Guangxi Medical University. The pangolins were seized by Chinese customs during anti-smuggling events from Southeast Asian countries and were maintained in the Wildlife Medical-aid and Monitoring Epidemic Diseases Research Center. Pangolin samples were transported and stored following standard procedures at Wuhan Institute of Virology, Chinese Academy of Sciences. The samples were stored in a -80°C freezer until further processing. The swab samples were centrifuged at $20,000 \times g$ for 10 min and 200 μL of the supernatant was subjected to RNA extraction using the QIAamp 96 Virus QIAcube HT Kit (Qiagen) according to the manufacturer's instructions. Samples were detected using pan-CoV detection primers targeting a 440-nt fragment in the *RdRp* gene of known alpha- and betacoronaviruses by one-step hemi-nested reverse transcription PCR (RT-PCR), as described previously.⁴⁰ The samples that tested positive in pan-CoV PCR detection were further processed for NGS using the QIAamp Viral RNA Mini Kit following the manufacturer's instructions. An unpurified RNA library (i.e., without removing host RNA) was constructed using the TruSeq Stranded mRNA Library Preparation Kit (Illumina). Paired-end (150-bp) sequencing of the RNA library was performed on the MGI DNBSEQ-T7 platform (v2.0). Cutadapt (v1.18) was used to remove low-quality reads with a minimum length of 30 bp and other parameters at default settings. MEGAHIT (v1.2.9) was used to assemble reads into contigs with minimum length of 500 bp and other parameters at default settings. Target contigs were selected using Blastn (v2.12.0+) searches against a local Coronaviridae database. Rough genomes were acquired using Geneious (v11.0.3) with medium sensitivity and other parameters at default settings following RACE and Sanger sequencing to obtain the complete genomes. RACE was performed using the SMARTER RACE 5'/3' Kit (Takara) as described previously.⁵¹

Serological tests

For MjHKU4r-CoV-1 NP antibody detection in pangolin serum samples, a LIPS assay was performed as described previously.⁵¹ In brief, the MjHKU4r-CoV-1 *N* gene was cloned into the pREN2 vector containing the *Renilla* luciferase gene. The pREN2-N plasmid was transfected into HEK293 cells and cell lysates were collected at 48 h post transfection (h.p.t.). For testing pangolin serum samples, 1 μL of serum was incubated with 10 million units of RLuc-N and 6 μL of 30% protein A/G UltraLink resin suspension (Pierce/Thermo Fisher Scientific). After washing to remove unbound luciferase-tagged antigens, the amount of NP captured was determined by measuring the luciferase signal using a commercial luciferase substrate kit (Promega). Microneutralization tests were performed to detect neutralizing antibody against MjHKU4r-CoV-1. MjHKU4r-CoV-1 (100 TCID₅₀) was pre-incubated with 1:10 or/and 1:20 diluted sera at 34°C for 1 h and then used to infect a monolayer of Caco-2 cells at 34°C for 1 h. Then, the serum-virus mixture was removed and cells were washed with Dulbecco's modified Eagle's medium (DMEM; Gibco) once. Fresh DMEM containing 2% fetal bovine serum (FBS) and one dose of antibiotic-antimycotic (Gibco) was added to the cells. At 72 h.p.i., the neutralizing effect was observed as the cytopathic effect (CPE) and using immunofluorescence (IF) staining. IF staining was quantified using ImageJ (v1.53c).

Virus isolation

Caco-2 cell monolayers were maintained in DMEM supplemented with 10% FBS (Gibco). Anal swab samples from pangolins that had tested positive for coronavirus by PCR were centrifuged and diluted in DMEM. The Caco-2 cells were inoculated with 200 μL of diluted sample or DMEM in a 5% CO₂ humidified incubator at 34°C for 1.5 h. Fresh DMEM containing 2% FBS containing double the dose of antibiotic-antimycotic (Gibco) was added to a final volume of 1 mL without removing the inoculum. The cells were incubated in the 5% CO₂ incubator at 34°C and observed daily for CPE. Virus was tittered using a Caco-2 cell-based infectivity assay and expressed as TCID₅₀/mL.

High-throughput sequencing, genome alignment, and metagenomics analysis of cultured viruses

High-throughput sequencing and data analysis were performed as described previously.² Briefly, culture supernatants from anal swab sample-inoculated Caco-2 cells were subjected to RNA extraction followed by NGS using a BGI MGISEQ2000 sequencer. The NGS reads were assembled into genomes using Geneious (v11.0.3). Metagenomics analysis was carried out mainly based on the bioinformatics platform MGmapper (PE_2.24 and SE_2.24). The raw NGS reads were first processed using Cutadapt (v1.18) with minimum read length of 30 base pairs. Burrows-Wheeler Aligner (v0.7.12-r1039) was used to align reads to a local database with a filter hits parameter at 0.8 FMM value and minimum alignment score at 30. For post-processing of assigned reads,

minimum size normalized abundance was set at 0.01, minimum read count at 20, and other parameters were default. The metagenomics analysis results were displayed in pie charts using Office 2010.

Phylogenetic analysis

Sequence alignment was carried out using Mega (v7.0.18) and BioEdit (v7.1.3.0). Sequences were aligned using mafft (v7.407) with default parameters. Phylogenetic trees were constructed by IQ-TREE (v1.6.1) with the HKY substitution model and 1,000 bootstrap replicates and edited with figtree (v1.4.3).

Transmission electron microscopy

Viral culture supernatant was fixed with 1% formaldehyde at 34°C overnight and then concentrated by ultracentrifugation through a 30% sucrose cushion at 140,000 × *g* at 4°C for 150 min using a SW28 rotor (Beckman). The pelleted viral particles were suspended in 100 μL of PBS, stained with 2% phosphotungstic acid (pH 7.0), and examined using a Tecnai transmission electron microscope (FEI) at 200 kV.

Immunofluorescence staining

Cells were washed with PBS twice and fixed with 4% paraformaldehyde at room temperature for 40 min. Viral NP expression was detected using an in-house rabbit polyclonal antibody against the *Tp* bat coronavirus HKU4 NP as a primary antibody and a Cy3-conjugated goat anti-rabbit IgG (Abcam, 1:200) as a secondary antibody. DPP4 expression was detected using DYKDDDDK-Tag (3B9) mouse monoclonal antibody (Abmart, 1:1,000) followed by Alexa Fluor 488-conjugated goat anti-mouse IgG (Abcam, 1:100). Nuclei were stained with DAPI (5 ng/mL). Staining patterns were examined using a fluorescence microscope (Thermo Fisher Scientific) or a confocal microscope (Nikon).

RNA extraction and quantitative real-time PCR

Viral RNA was extracted from culture supernatants using the QIAamp Viral RNA kit (Qiagen) or DNA/RNA Extraction Kit (Prepackaged, Vazyme) according to the manufacturer's instructions. Total RNA samples were prepared from organoids or explants using TRIzol Reagent (Invitrogen). Viral RNA concentration was determined by one-step quantitative reverse transcription PCR (qRT-PCR) using primers targeting MjHKU4r-CoV-1 ORF5 (forward: 5'-CTTCGTGTTGATAATGGTACTTCC-3', reverse: 5'-AGCAGAGTGCACATAGAAACA-3') or MERS-CoV NP (forward: 5'-GGGTGTACCTCTTAATGCCAATTC-3', reverse: 5'-TCTGTCCTGTCTCCGC CAAT-3'). One step qRT-PCRs were run using the HiScript II One Step qRT-PCR SYBR Green Kit (Vazyme) on a CFX Connect Real-Time PCR Detection System (Bio-Rad). Viral sequence copies were determined by comparing the Ct values to a standard curve derived from a cDNA clone. Total RNA was extracted by using RNeasy Pure Cell/Bacteria Kit (TIANGEN) and reverse transcript to cDNA by HiScript II 1st Strand cDNA Synthesis Kit (Vazyme). cDNAs were prepared for real time PCR by using Taq Pro Universal SYBR qPCR Master Mix (Vazyme).

Western blotting

Cells were lysed and total proteins were separated by 10% sodium dodecyl sulfate-polyacrylamide gel electrophoresis and then transferred onto a polyvinylidene difluoride membrane (Millipore). The membrane was incubated with the indicated primary antibodies at 4°C overnight and the indicated secondary antibodies at room temperature for 1 h. The signals were detected using Immobilon western horseradish peroxidase substrate (Millipore). For the detection of hDPP4 protein in Huh-7 cells, the membrane was incubated with goat anti-hDPP4 polyclonal antibody (R&D, 0.3 μg/mL) and detected with horseradish peroxidase-conjugated rabbit anti-goat IgG (Proteintech, 1:5,000). For the detection of full and cleaved S protein, the membrane was incubated with mouse anti-Stag monoclonal antibody (1:5,000) and detected with horseradish peroxidase-conjugated goat anti-mouse IgG (Proteintech, 1:10,000). For the detection of VSV matrix protein, the membrane was incubated with mouse anti-VSV M monoclonal antibody (Ferafast, 1:1,000) and detected with horseradish peroxidase-conjugated goat anti-mouse IgG (Proteintech, 1:10,000). For the detection of human GAPDH protein, the membrane was incubated with mouse monoclonal antibody (Proteintech, 1:10,000) and detected with horseradish peroxidase-conjugated goat anti-mouse IgG (Proteintech, 1:10,000).

Establishment of the hDPP4-knockout cell line

hDPP4-knockout cell lines were established using the CRISPR/Cas9-editing system. A single-guide RNA (5'-CACCGCACCATCATC ACCGTGCCCG-3') targeting exon 2 of *hDPP4* was cloned into the lentiCRISPR-v2 vector (a kind gift from Prof. Lin-Fa Wang, Duke-NUS Medical School) at the *BsmBI* site. The construct was co-transfected with three packaging plasmids (pMD2.G, pMDLg/PRRE and pRSV/Rev, kind gifts from Prof. Lin-Fa Wang, Duke-NUS Medical School) and Fugene6 (Promega) into HEK293 cells to produce lentiviruses. Huh-7 cells were lentivirally transduced and then selected on 7 μg/mL puromycin for one week. Surviving cells were diluted and seeded into 96-well plates for clonal expansion. Successful *hDPP4* knockout was verified using Sanger sequencing and western blotting.

Construction of plasmids expressing DPP4 orthologues

Coding sequences of *Pipistrellus pipistrellus* bat DPP4 (*PpDPP4*, GenBank: KC249974.1), *Manis javanica* pangolin DPP4 (*MjDPP4*, XM_017664375.2), ferret DPP4 (KF574264.1), pig DPP4 (NM_214257.1), goat DPP4 (KF574265.1), cat DPP4 (NM_001009838.1),

rabbit DPP4 (XM_008258668.2), horse DPP4 (XM_023623018.1), rat DPP4 (NM_012789.2), macaque DPP4 (NM_001039190.2), sheep DPP4 (XM_004004660.5), hamster DPP4 (NM_001310571.1), camel DPP4 (KJ002534.1), marmoset DPP4 (XM_002749392), cattle DPP4 (NM_174039.3), dog DPP4 (XM_038463398.1) and mouse DPP4 (NM_001159543.1) were synthesized and cloned into pCMV-3Tag-8 vector. hDPP4 and *Tylonycteris pachypus* bat DPP4 (*TpDPP4*) were amplified and cloned into the same vector. Purified DPP4 plasmids were transfected into HeLa cells. Expression of DPP4 protein was confirmed by immunofluorescence assay (IFA) with DYKDDDDK-Tag (3B9) mouse monoclonal antibody (Abmart, 1:1,000). To transiently express hDPP4 protein in Huh-7 knockout cells, the hDPP4 coding sequence with an S-tag and synonymous mutations in gRNA target sequences were amplified and cloned into the pQCXIH vector, and DPP4 protein expression was confirmed by western blotting using the antibody against S-tag (1:5,000).

RBD and DPP4 protein expression and purification

The constructs used for protein expression and purification were respectively cloned by insertion of the codon-optimized sequences for MERS-RBD (S residues E367–Y606, GenBank: AFS88936.1), HKU4-RBD (S residues E372–Y611, ABN10848.1), and MjHKU4-CoV-1-RBD (S residues E375–Y614), or the original coding sequences for hDPP4 (residues S39–D496), *TpDPP4* (residues S38–N493), *PpDPP4* (residues T36–N490, AGF80256.1), and *MjDPP4* (residues S39–D496, XP_017519864.1) into the pcDNA3.1 or pCAGGS vector, with an N-terminal signal peptide and a C-terminal S-tag to facilitate protein secretion and purification. For protein expression, HEK293F cells were transiently transfected with the above constructs using polyethylenimine (Polysciences) and then cultured in FreeStyle 293 Expression Medium (Gibco) in a humidified 5% CO₂ superposition thermostatic oscillator at 37°C. At 72 h.p.t., supernatants were harvested and centrifuged to remove cell debris. The clarified supernatants were used for protein purification with S-tag agarose beads. Purified proteins were quantified using a Qubit 2.0 Fluorometer (Thermo Fisher Scientific).

Biolayer interferometry

The affinity between RBD and DPP4 proteins was evaluated using the Octet RED system (ForteBio) in 96-well microplates at 30°C under shaking at 1,000 rpm. RBD proteins were biotinylated with EZ-Link NHS-LC-LC-Biotin (Thermo Fisher Scientific). The streptavidin biosensors were activated for 200 s, followed by coupling with 40 µg/mL biotinylated RBD for 600 s. A baseline was collected in kinetic buffer (150 mM NaCl, 10 mM HEPES, and 0.005% Tween-20; pH 7.2) for 200 s. The RBD-loaded biosensors were immersed in DPP4 proteins with a series of twofold dilutions for 900 s and then dissociated in the same kinetic buffer for another 900 s. Data were analyzed after correction by subtracting the value of a reference sample. A 1:1 binding model with global fit was applied to all data using Data Analysis v6.4 (ForteBio). The coefficient of determination (R^2) for the interactions was close to 1.0.

Pseudovirus production and transduction

MERS-CoV- and wild-type- and mutant-MjHKU4r-CoV-1- or HKU4-CoV-S-packaged pseudovirus particles were generated in HEK293 cells. pcDNA3.1 vectors containing MERS-CoV-S, MjHKU4r-CoV-1-S (wild-type) or mutated S (₆₃₄RQQR₆₃₇ to ₆₃₄AQQA₆₃₇), or HKU4-CoV-S were respectively transfected into HEK293 cells using Lipofectamine 3000 transfection reagent (Invitrogen) according to the manufacturer's instruction. Empty vector was transfected as a control. At 24 h.p.t., the cells were transduced with VSV-ΔG-Fluc. After 2 h, the inoculum was removed and the cells were washed with DMEM and then added with medium containing VSV-G antibody (Kerafast, 1:1,000). The supernatant containing pseudoviruses was harvested at 48 h post transduction, and cell debris was removed by centrifugation and filtration. Huh-7 and Caco-2 cells were transfected with pseudoviruses and harvested to determine luciferase activity using a Luciferase Assay System and a GloMax luminometer (Promega). Pseudovirus was quantified as previously described.⁵² Briefly, viral RNA was extracted and subjected qRT-PCR. The P protein gene of VSV virus was quantified and viral copy number was calculated. The primers used were: forward: 5'-TCTCGTCTGGATCAGGCGG-3'; reverse: 5'-TGCTCTTCCACTCCATCCTCTTGG-3'. All pseudoviruses were normalized to the same amount before transduction.

Protease inhibition

Huh-7 cells were incubated with 10 µM decanoyl-RVKR-CMK (Tocris), 50 µM Camostat (MedChemExpress), or 50 µM E64D (Selleck) for 2 h before infection. Equal volumes of water and dimethylsulfoxide (DMSO) served as vehicle controls. After the 2-h pretreatment, the media containing inhibitors and control media were removed. The Huh-7 cells were infected with MjHKU4r-CoV-1 at a multiplicity of infection (MOI) of 10 in a 5% CO₂ incubator at 34°C for 8 h and then fixed with 4% paraformaldehyde and subjected to IF staining.

Human organoid infection, viral load determination, and IF staining

Human adult distal lung and colon biopsies were obtained and used for research purposes with approval from the Medical Ethical Council of Tongji Hospital. The study adhered to the principles of the Declaration of Helsinki. For preparing human airway organoids, we followed the protocol described by Sachs et al.,⁵³ with modification. In brief, after washing with cold PBS, the lung tissue was minced into ~2-mm-thick sections and incubated with 400 U/mL collagenase (Gibco) mixed with airway organoid medium at 37°C for 1–2 h. The suspension was strained through a 100-µm cell filter (Falcon). To end the digestion, 2% FBS was added to the suspension. Then, the suspension was centrifuged at 250 × g for 3 min. The pelleted lung cells were resuspended in cold Matrigel and seeded in 24-well plates. After the Matrigel was solidified, 500 µL of airway organoid medium was added to each well, and the plates were transferred to a humidified 5% CO₂ incubator at 37°C. The medium was changed every 4 days and organoids were passaged every 2 weeks.

Human colon organoids were prepared according to the protocol reported by Sato et al.,⁵⁴ with modification. Briefly, the tissue was washed with cold PBS until the supernatant was clear. Subsequently, the tissue was cut into small fragments and incubated with 5 mM EDTA in PBS at 4°C for 30–40 min. After removing the EDTA buffer, the tissue fragments were resuspended in cold PBS and the suspension was pipetted up and down several times to isolate the crypts. Then, the suspension was stained through a 70- μ m cell filter (Falcon). After centrifugation at 250 \times *g* for 3 min, the pelleted cells were embedded in Matrigel and seeded in 24-well plates. After the Matrigel was solidified, 500 μ L of colon organoid medium was added to each well, and the plates transferred to a humidified 5% CO₂ incubator at 37°C. The medium was changed every 3 days and organoids were passaged every 2 weeks.

For organoid infection, organoids were infected with MjHKU4r-CoV-1 or DMEM at 34°C for 2 h after removing the Matrigel from the organoids. The infection was performed at a MOI of 1 for viral replication determination and a MOI of 3 for IF staining. After incubation, the organoids were washed once with PBS and centrifuged at 250 \times *g* for 3 min. The organoid pellets were embedded in Matrigel and seeded in a 24-well plate. After polymerization, culture medium was added. At the indicated time points, organoids and culture media were harvested for RNA extraction and viral load quantification by qRT-PCR. Culture media were also used for authentic virus load quantification by the TCID₅₀ assay.

For IF staining, the organoids were removed from the Matrigel and fixed with 4% paraformaldehyde at 4°C for 24 h. After washing with PBS, the organoids were permeabilized with 0.25% Triton X-100 (Sigma) in PBS for 30 min, washed with PBST (0.1% Tween-20) three times, and blocked in 5% BSA for 1 h. The organoids were incubated with the indicated primary antibodies at 4°C overnight, washed with PBST three times, and incubated with the indicated secondary antibodies and DAPI at room temperature for 1 h. Finally, the organoids were imaged under a confocal microscope (Olympus, FV3000).

Human tissue *ex vivo* infection, viral load determination, and IF staining

Human colon tissues were collected from patients with non-infectious disease who underwent surgical resection after obtaining written consent from them with approval from the Medical Ethical Council of Tongji Hospital. For viral infection in *ex vivo* cultures, full-thickness tissues were cut into tiny strips and positioned in a 24-well culture plate. The tissue strips were incubated with 10⁶ TCID₅₀ of virus or DMEM in a volume of 1 mL at 34°C for 2 h. After the inoculation, the *ex vivo* tissue strips were rinsed with DMEM and cultured in 500 μ L of Ham's F-12K (Gibco) medium containing one dose of antibiotic-antimycotic (Gibco) in a 5% CO₂ incubator at 34°C. At the indicated time points, the tissue strips and culture media were harvested for RNA extraction and quantification of viral load by qRT-PCR. For IF staining, the tissue strips were collected and fixed with 4% paraformaldehyde at 4°C for 24 h, embedded in paraffin, and cut into 4- μ m sections. For IF staining, the sections were deparaffinized, rehydrated, and subjected to heat-induced antigen retrieval. After permeabilization with 0.2% Triton X-100 (Sigma), the sections were blocked with 5% BSA for 1 h and incubated with the indicated primary antibodies at 4°C overnight and then with the relevant secondary antibodies and DAPI at room temperature for 1 h. Tissue imaging was performed using a confocal microscope (Nikon).

Mouse infection

Seven to fourteen-week-old hDPP4-Tg mice were anesthetized with tribromoethanol (Avertin) (250 mg/kg) and infected intranasally with 1 \times 10⁶ TCID₅₀ MjHKU4r-CoV-1 in 20 μ L of DMEM (for the virus-challenged group) or with the same volume of DMEM (for the mock-infected group). Mice were observed for clinical signs and weighed daily. Four mice (male and female) were euthanized at 1, 3, and 5 d.p.i. and all mice were euthanized at the end of the experiment, and lung and brain tissues were harvested for the determination of viral loads and histological analysis.

Histological analysis

Lung and brain samples harvested at the indicated time points were fixed with 4% paraformaldehyde, embedded in paraffin, and cut into 4- μ m sections. For routine histology, the tissue sections were stained with hematoxylin-eosin. To detect virus N antigen, IF staining was performed using rabbit polyclonal antibody anti-MjHKU4r-CoV-1 NP (1:800) as a primary antibody and Cy3-conjugated goat anti-rabbit IgG (Abcam, 1:200) as a secondary antibody. IF staining was performed as described above. Imaging data were collected using a Panoramic MIDI system (3DHISTECH).

IFN-I production and signaling luciferase reporter assays

HEK293 cells were co-transfected with 10 ng of IFN- β promoter reporter plasmid, 4 ng *Renilla* luciferase plasmid, 4 ng RIG-I (2CARD) stimulator expressing plasmid, and 86 ng of viral protein expression plasmid or empty vector using Lipofectamine 3000 transfection reagent. At 24 h.p.t., the cells were assayed for dual-luciferase activities. For the IFN-I signaling, HEK293 cells were co-transfected with 90 ng of ISRE promoter reporter plasmid, 10 ng of *Renilla* luciferase plasmid, and 100 ng of viral protein expression plasmid. At 16 h.p.t., the transfected cells were treated with 500 units/mL of Universal Type I IFN Protein. After another 8 h incubation, the cells were lysed and performed dual-luciferase reporter assays. Luciferase signals were measured by GloMax (Promega).

Antiviral assays

Remdesivir (Selleck, S8932), GC376 (Selleck, S0475), EIDD-2801 (Selleck, S8969) were purchased from Selleck Chemicals. Antiviral efficacy assays were performed in Caco-2 cells. Cells were plated in a 96-well plate, cultured overnight, and inoculated with MjHKU4r-CoV-1 or MERS-CoV at a MOI of 0.01 for 1 h in the presence of a serial dilutions of each drug. One hour after inoculation,

the virus was removed, the cells were washed with DMEM once, and fresh medium containing dilutions of each drug was added to the cells. At 72 h.p.i., culture supernatants were collected and viral RNA was extracted for the quantification of viral genomic copies by qRT-PCR.

Viral neutralization assessment by fluorescence reduction neutralization assay

The neutralization efficacy of neutralizing antibodies was assessed using a fluorescence reduction neutralization assay. Neutralizing antibodies were serially diluted two-fold and incubated with 100 TCID₅₀ of virus at 34°C for 1 h. The virus-antibody mixture was then transferred to a 96-well plate with Caco-2 cell monolayers in triplicate. After a 1-h incubation, the virus-antibody mixture was removed. The cells were washed with DMEM once and fresh DMEM containing 2% FBS and one dose of antibiotic-antimycotic (Gibco) was added. At 24 h.p.i., the cells were fixed with 4% paraformaldehyde at room temperature for 40 min and then subjected to IF staining. The plates were read and nuclei and NP positive cells were quantified using an Operetta high-content imaging system (PerkinElmer). Virus-only infected cells were assayed as a control.

Biosafety and biosecurity

All experiments involving MjHKU4r-CoV-1 and MERS-CoV were performed in certified BSL3 laboratories in biological safety cabinets using standard operating procedures that were reviewed and approved by the Institutional Biosafety Committees of Wuhan Institute of Virology, Chinese Academy of Sciences (permit number: WIV/B3/05/202001).

QUANTIFICATION AND STATISTICAL ANALYSIS

Data are presented as means and standard errors of the means (SEMs) of at least triplicate measurements. Statistical significance was assessed using a two-tailed Student's *t*-test or two-way ANOVA in GraphPad Prism 8. *P* < 0.05 was considered statistically significant. **P* < 0.05; ***P* < 0.01; ****P* < 0.001; *****P* < 0.0001; ns, no significant difference.

Supplemental figures

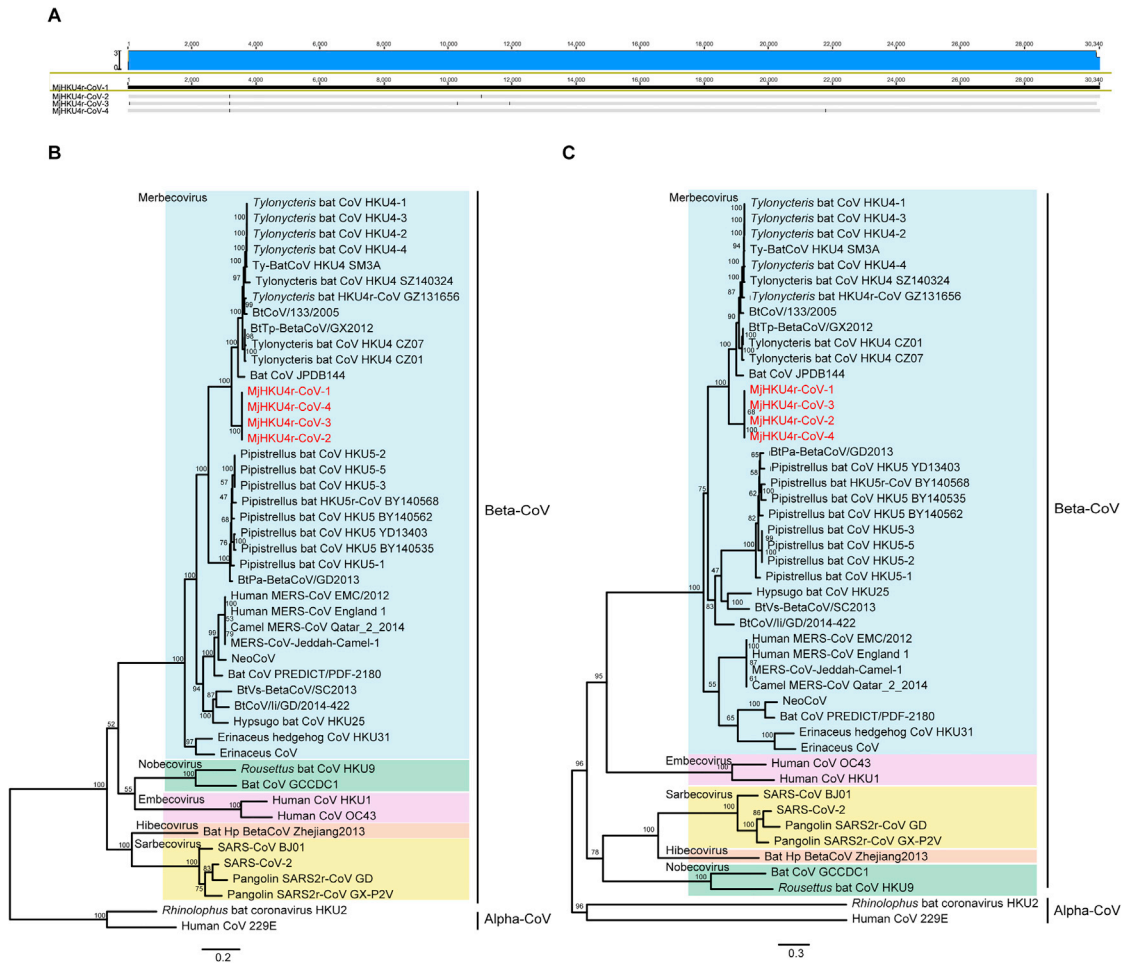


Figure S1. Genome characterization and phylogenetic analysis of MjHKU4r-CoV, related to Figure 1

(A) MjHKU4r-CoV-2, -3, and -4 genome sequences mapped to the reference sequence, MjHKU4r-CoV-1. SNPs are displayed on the genomes.

(B and C) Phylogenetic trees based on the *RdRp* nucleotide sequences (B) or complete *S* gene nucleotide sequences (C) of representative Alpha and Beta coronaviruses. MjHKU4r-CoVs are shown in red. Different color shades represent different subgenera of coronaviruses. The scale bars represent 0.2 or 0.3 substitutions per nucleotide position. The software and setting used are described in the [STAR Methods](#).

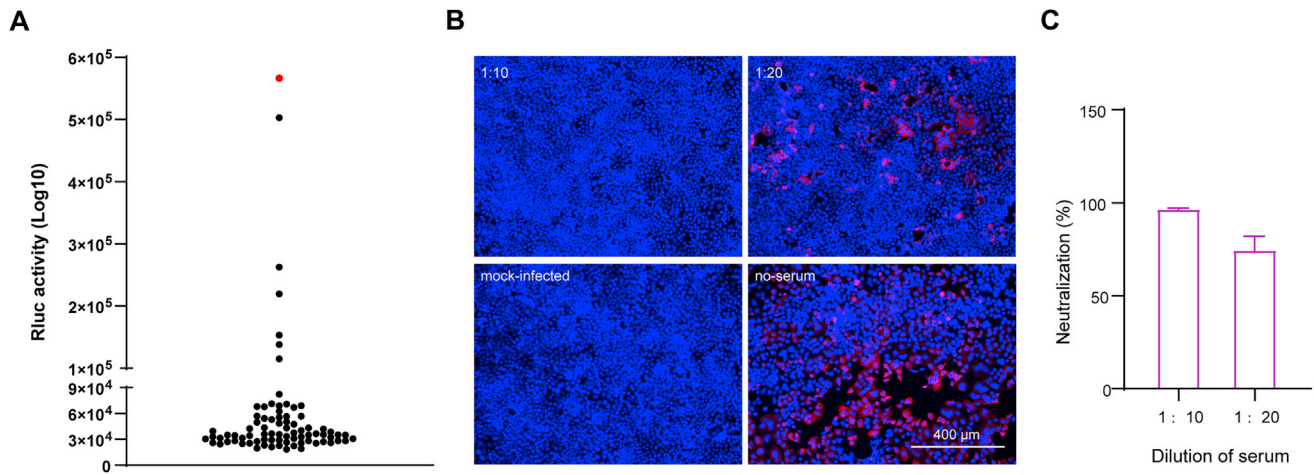
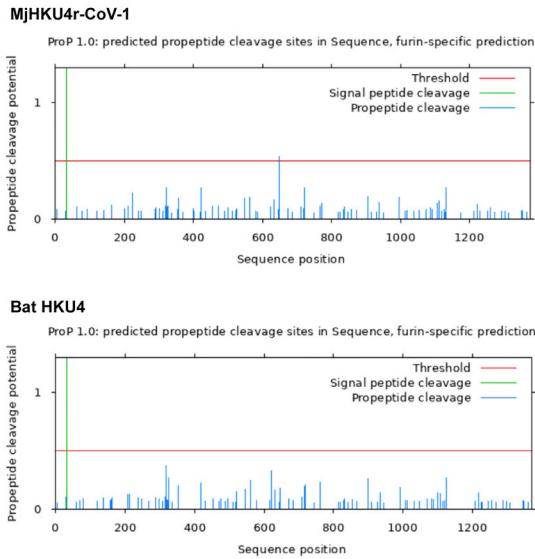


Figure S2. Serological investigation through LIPS and microneutralization test (MNT) assays, related to Figure 1

(A) MjHKU4r-CoV NP antibodies in 80 pangolin serum samples were detected using LIPS (the only positive sample in the MNT assay is shown in red).

(B and C) Pangolin sera were tested for neutralizing antibodies against MjHKU4r-CoV-1 by the MNT assay at 1:10 and 1:20 dilutions. IF staining of a pangolin serum sample positive for neutralization antibody at 1:10 and 1:20 dilutions is shown. Mock-infected and no-serum infection were included as controls (B). Neutralizing activity was quantified using ImageJ (C).

A



B

Pangolin			
	MjHKU4r-CoV-1	628 - C T A V G I R Q Q R F V Y D S F -	643
	MjHKU4r-CoV-2	628 - C T A V G I R Q Q R F V Y D S F -	643
	MjHKU4r-CoV-3	628 - C T A V G I R Q Q R F V Y D S F -	643
	MjHKU4r-CoV-4	628 - C T A V G I R Q Q R F V Y D S F -	643
	Bat HKU4-1	625 - C T A V G V K Q Q R F V Y D S F -	640
	Bat HKU4-2	625 - C T A V G V K Q Q R F V Y D S F -	640
	Bat HKU4-3	625 - C T A V G V K Q Q R F V Y D S F -	640
	Bat HKU4-4	625 - C S A V G V K Q Q R F V Y D S F -	640
	BITp-BetaCoV/GX2012	625 - C T A V G V K Q Q R F V Y D S F -	640
	BTCoV/133/2005	625 - C T A V G V K Q Q R F V Y D S F -	640
	Bat HKU4r-CoV GZ1316656	625 - C S A V G I K Q Q R F V Y D S F -	640
	Bat HKU4 isolate SZ140324	625 - C T A V G V K Q Q R F V Y D S F -	640
	Bat HKU4 isolate CZ01	625 - C T A V G V K Q Q R F V Y D S F -	640
	Bat HKU4 isolate CZ07	625 - C T A V G V K Q Q R F V Y D S F -	640
	Bat HKU4 isolate SM3A	625 - C S A V G V K Q Q R F V Y D S F -	640
	Bat HKU4 isolate GZ1707	625 - C T A V G V K Q Q R F V Y D S F -	640
	Bat HKU4 isolate GZ1708	625 - C T A V G V K Q Q R F V Y D S F -	640
	Bat HKU4 isolate GZ1709	625 - C T A V G V K Q Q R F V Y D S F -	640
	Bat HKU4 isolate GZ1823	625 - C T A V G V K Q Q R F V Y D S F -	640
	Bat HKU4 isolate GZ1824	625 - C T A V G V K Q Q R F V Y D S F -	640
	Bat HKU4 isolate GZ1829	625 - C T A V G V K Q Q R F V Y D S F -	640
	Bat HKU4 isolate GZ1830	625 - C T A V G V K Q Q R F V Y D S F -	640
	Bat HKU4 isolate GZ1832	625 - C T A V G V K Q Q R F V Y D S F -	640
	Bat HKU4 isolate GZ1857	625 - C T A V G V K Q Q R F V Y D S F -	640
	Bat HKU4 isolate GZ1858	625 - C T A V G V K Q Q R F V Y D S F -	640
	Bat HKU4 isolate GZ1859	625 - C T A V G V K Q Q R F V Y D S F -	640
	Bat HKU4 isolate GZ1861	625 - C T A V G V K Q Q R F V Y D S F -	640
	Bat HKU4 isolate GZ1862	625 - C T A V G V K Q Q R F V Y D S F -	640
	Bat HKU4 isolate GZ1863	625 - C T A V G V K Q Q R F V Y D S F -	640
	Bat HKU4 isolate GZ1864	625 - C T A V G V K Q Q R F V Y D S F -	640
	Bat HKU4 isolate GZ1907	625 - C T A V G V K Q Q R F V Y D S F -	640
	Bat HKU4 isolate GZ1912	625 - C T A V G V K Q Q R F V Y D S F -	640
	Bat HKU4 isolate GZ1919	625 - C T A V G V K Q Q R F V Y D S F -	640
	Bat HKU4 isolate GZ190421	625 - C T A V G V K Q Q R F V Y D S F -	640
	Bat HKU4 isolate 2S	625 - C T A V G V K Q Q R F V Y D S F -	640
	Bat HKU4 isolate 3S	625 - C S A V G V K Q Q R F V Y D S F -	640
	Bat HKU4 isolate 4S	625 - C S A V G V K Q Q R F V Y D S F -	640
	Bat HKU4 isolate 5S	625 - C S A V G V K Q Q R F V Y D S F -	640
	Bat HKU4 isolate 6S	625 - C S A V G V K Q Q R F V Y D S F -	640
	Bat HKU4 isolate 7S	625 - C S A V G V K Q Q R F V Y D S F -	640
	Bat HKU4 isolate 8S	625 - C S A V G V K Q Q R F V Y D S F -	640
	Bat HKU4 isolate 9S	625 - C S A V G V K Q Q R F V Y D S F -	640
	Bat HKU4 isolate 10S	625 - C S A V G V K Q Q R F V Y D S F -	640
	Bat HKU4 isolate 11S	625 - C S A V G V K Q Q R F V Y D S F -	640
	Bat HKU4 isolate 12S	625 - C S A V G V K Q Q R F V Y D S F -	640
	Bat HKU4 isolate 14S	625 - C S A V G V K Q Q R F V Y D S F -	640
	Bat HKU4 isolate 15S	625 - C S A V G V K Q Q R F V Y D S F -	640
	Bat CoV isolate JPDB144	625 - C S A V G V K Q Q R F V Y D S F -	640
	Bat CoV isolate 160079	625 - C T A V G V K Q Q R F V Y D S F -	640
	Bat CoV isolate 160081	625 - C T A V G V K Q Q R F V Y D S F -	640
	Bat CoV isolate 161028	625 - C T A V G V K Q Q R F V Y D S F -	640

Figure S3. Prediction and alignment of putative furin cleavage sites in pangolin MjHKU4r-CoV and bat HKU4r-CoVs, related to Figure 1

(A) Prediction of furin cleavage sites in the S proteins of MjHKU4r-CoV-1 and bat HKU4 was carried out using ProP-1.0 Server (<https://services.healthtech.dtu.dk/service.php?ProP-1.0>), using the furin-specific prediction as the default.

(B) Predicted furin cleavage site of MjHKU4r-CoV and the corresponding sites in all publicly available bat HKU4r-CoVs. The arginine sites are shown in red, and the predicted furin cleavage sites are gray shaded.

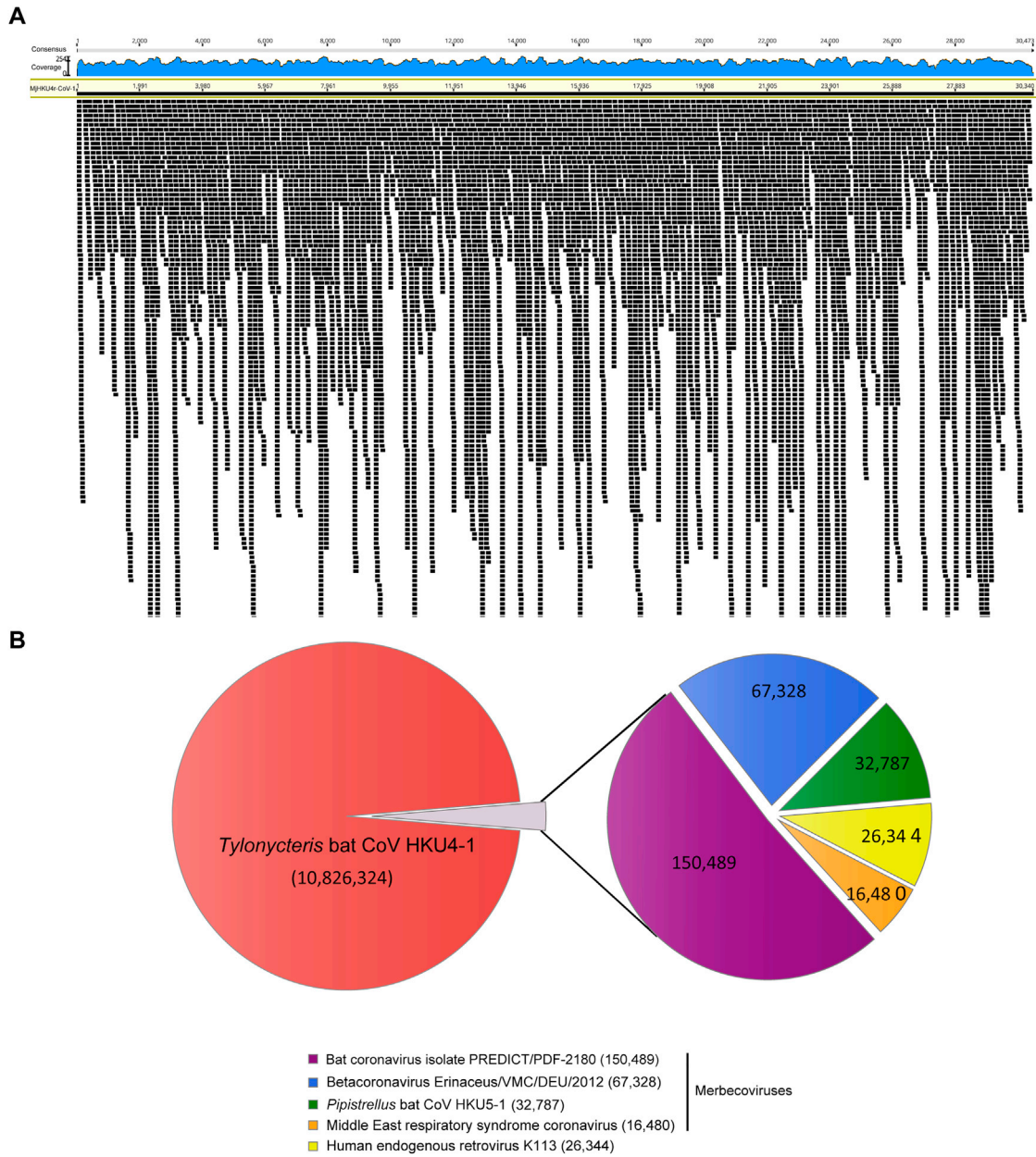


Figure S4. Mapping analysis of NGS raw reads and metagenomics analysis of MjHKU4r-CoV-1 cell culture, related to Figure 2

(A) High-throughput sequencing was performed using RNA extracted from supernatants of MjHKU4r-CoV-1-infected Caco-2 cell cultures. Reads randomly extracted from NGS raw data of isolated MjHKU4r-CoV-1 were mapped to the reference sequence obtained from an anal swab sample.

(B) Metagenomics analysis of sequencing data from MjHKU4r-CoV-1 viral supernatant.

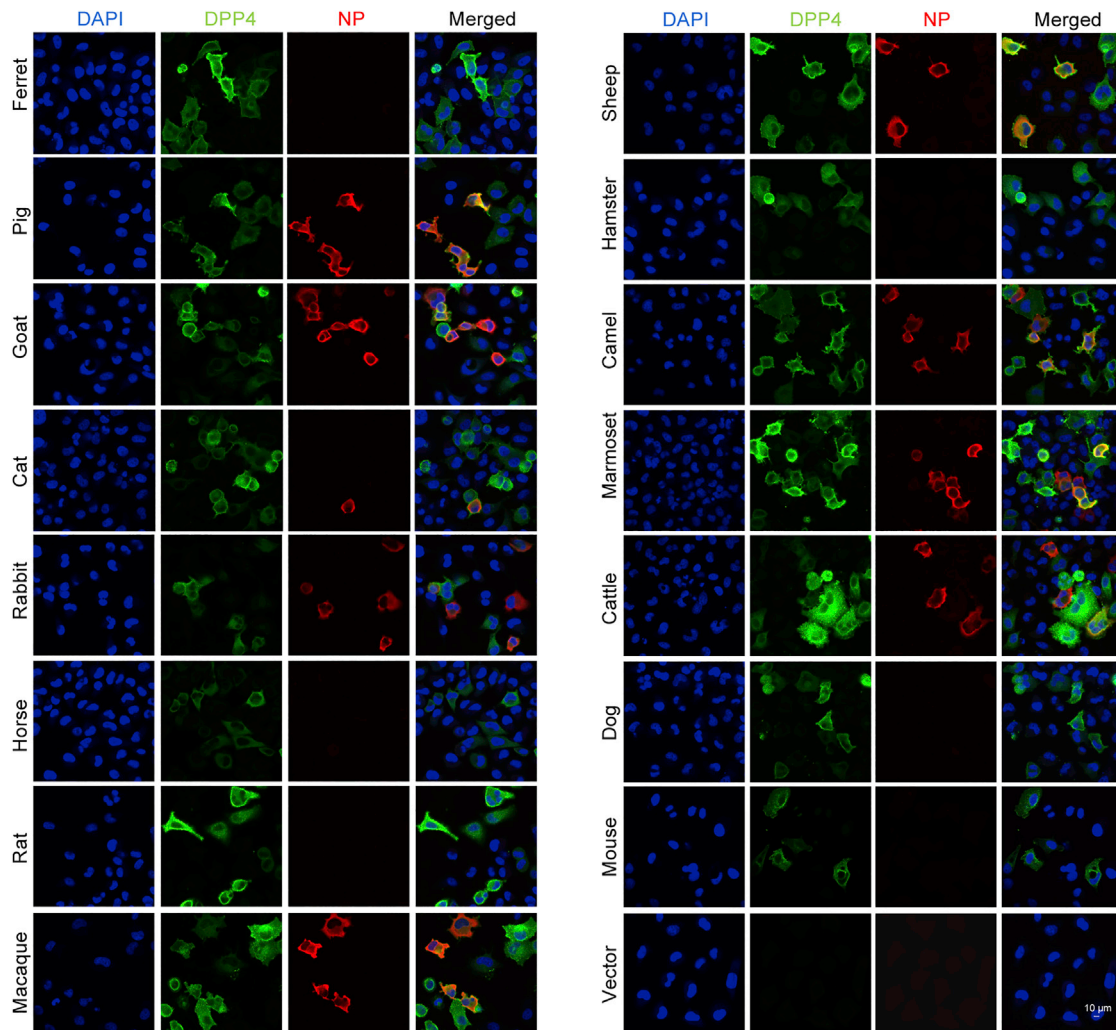


Figure S5. Functional assessment of different DPP4 orthologs mediating MjHKU4r-CoV-1 infection, related to Figure 4

HeLa cells overexpressing DPP4 orthologs from various mammals or empty vector were infected with MjHKU4r-CoV-1 (MOI = 1). At 24 h.p.i., the cells were fixed and subjected to IF staining. MjHKU4r-CoV-1 NP (red), DPP4 protein expression (green), and nuclei (blue) are shown (scale bars, 10 µm).

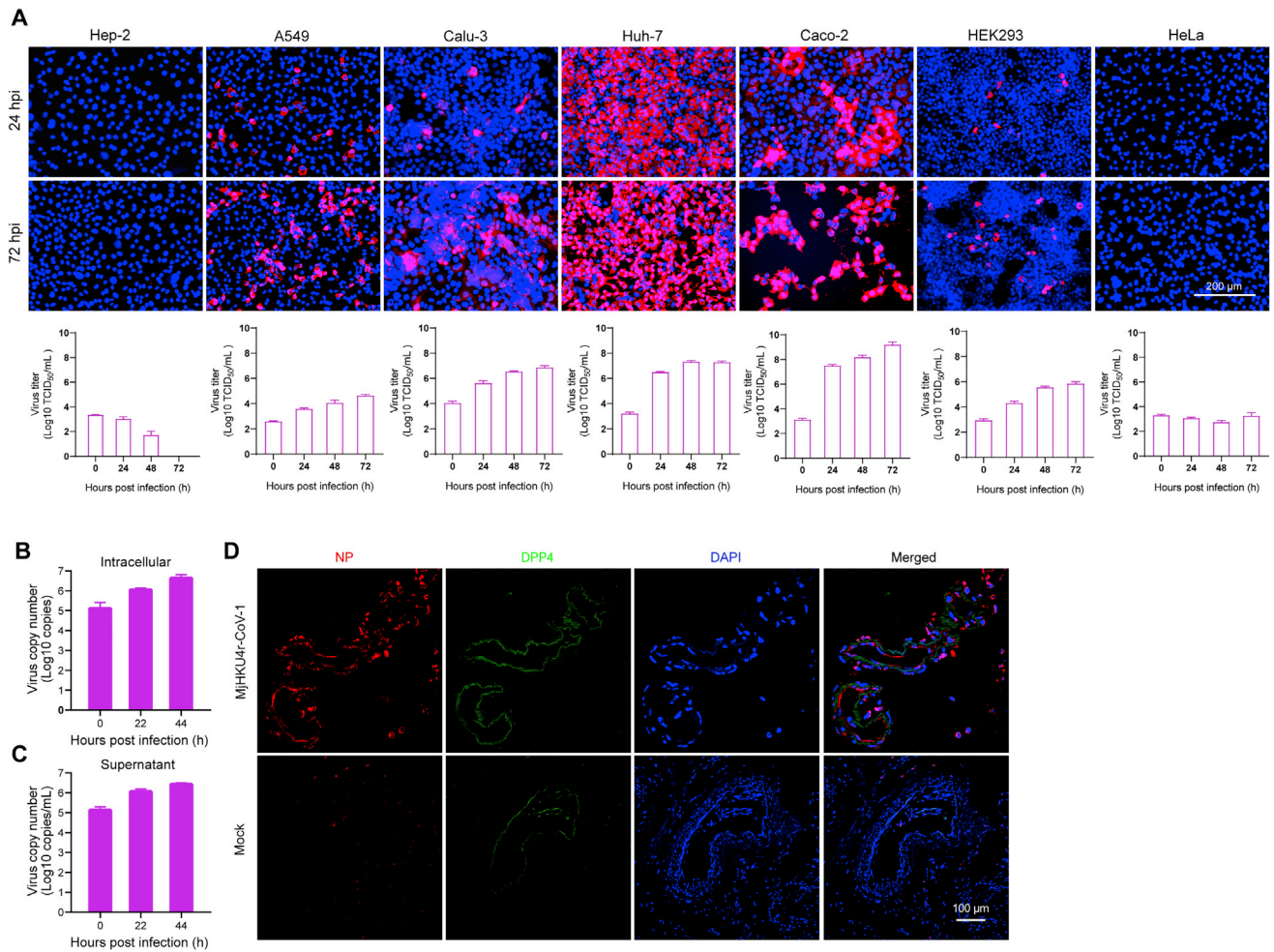


Figure S6. Human cell tropism and human colon *ex vivo* infection of MjHKU4r-CoV-1, related to Figure 5

(A) NP staining (red) of the indicated human cell lines at 24 h and 72 h.p.i. with MjHKU4r-CoV-1. Blue, nuclei; scale bars, 200 μm. Replication of MjHKU4r-CoV-1 in cell culture supernatant was analyzed by TCID₅₀ assay.

(B–D) qRT-PCR detection of the replication of MjHKU4r-CoV-1 in human *ex vivo* colon tissue (B) or culture supernatant (C). IF staining of human *ex vivo* colon at 24 h.p.i. with MjHKU4r-CoV-1 (D). Red, viral NP; green, human DPP4; blue, nuclei; scale bars, 100 μm.

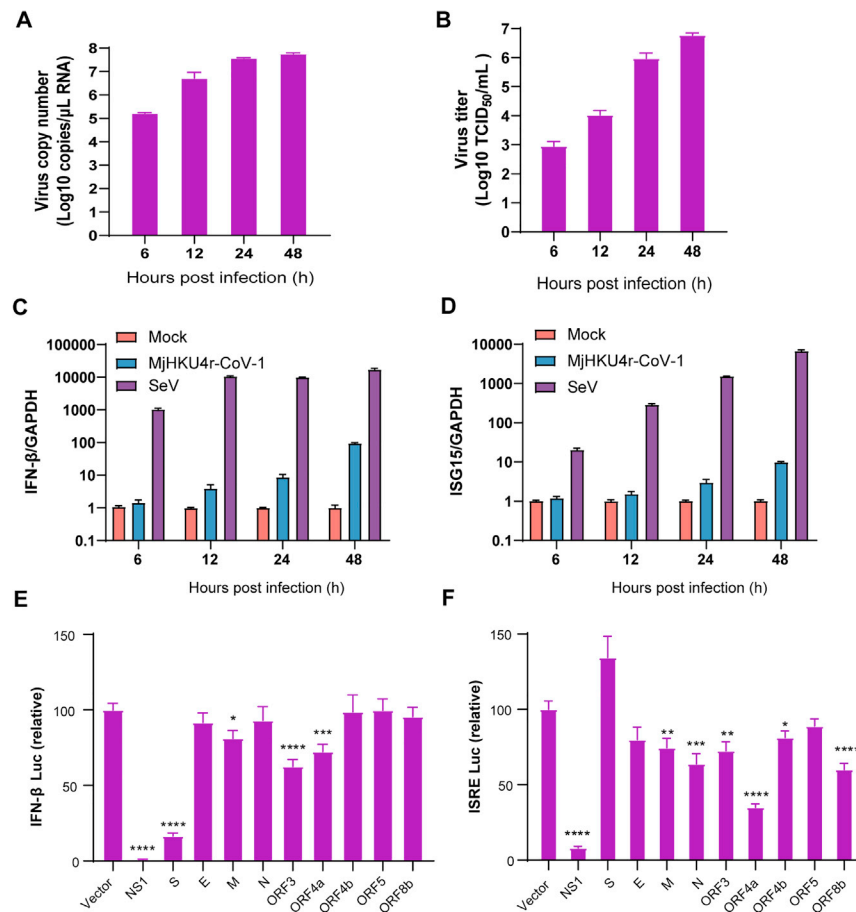


Figure S7. Evasion of the type I IFN response by MjHKU4r-CoV-1, related to Figure 6

(A and B) Caco-2 cells were infected with MjHKU4r-CoV-1 (at a MOI of 2). At 6, 12, 24, and 48 h.p.i., viral RNA copies in cell lysates were determined by qRT-PCR (A), and viral titers in the supernatant were determined by TCID₅₀ assay (B).

(C and D) Caco-2 cells infected with MjHKU4r-CoV-1 (at a MOI of 2), Sendai virus (100 hemagglutinating units/mL), or mock infected were collected at indicated times. Total RNA extracted from cells was used to evaluate *IFNB-β* (C) and *ISG15* (D) mRNA levels, shown as fold changes relative to the *GAPDH* level.

(E) HEK293 cells were co-transfected with viral protein expression plasmids or empty vector, simulator plasmid RIG-I (2CARD), firefly luciferase reporter plasmid pIFN-β-luc, and *Renilla* luciferase plasmid pRL-TK. At 24 h.p.t., luciferase activity was measured. Empty vector was set to 100%. NS1 protein of influenza A virus served as a positive control.

(F) HEK293 cells were co-transfected with viral protein expression plasmids or empty vector, firefly luciferase reporter plasmid pISRE-luc, and *Renilla* luciferase plasmid pRL-TK. At 24 h.p.t., the cells were treated with 500 U/mL universal IFN-α for another 8 h and luciferase activity was measured. Empty vector was set to 100%. NS1 protein of influenza A virus served as a positive control.

Data are presented as means and SEMs of at least triplicate measurements in (E) and (F). Statistical significance was assessed using a two-tailed Student's t test.